Building Calorimetric Detectors for CERN Experiments

Diploma Thesis

András LÁSZLÓ

Eötvös University, Budapest, Hungary

`laszloa@szofi.elte.hu`

Supervisor: György Vesztergombi

KFKI-RMKI, Budapest, Hungary

`veszter@rmki.kfki.hu`

2004

Abstract

In this paper, studies on two calorimetric detectors from CERN experiments are summarized.

The first detector is the HF (Hadronic Forward) calorimeter from the detector complex of CMS (Compact Muon Solenoid). Linearity and homogeneity tests were carried out on parts of this detector, which are evaluated in this paper.

The second detector is the LGC (Lead glass Gamma Calorimeter) from the experiment NA49. The detector is newly constructed: it was mounted and first brought into operation in October 2003. The main goal of these studies on LGC is to show the basic properties of the detector in operation. The main result is the π^0 mass peak, which is the first physical effect measured with the LGC.

Contents

Áttekintés

Ebben a dolgozatban CERN kísérletekhez készült két kalorimetrikus detektoron végzett vizsgálataimat foglalom össze. Az egyik detektor a HF (Hadronic Forward) kaloriméter, ami a CMS (Compact Muon Solenoid) detektorkomplexumhoz készül, amely a CERN-beli LHC (Large Hadronic Collider) részecskegyorsító mentén épül fel, nagyenergiás részecskefizikai mérésekhez. A másik detektor az LGC (Lead glass Gamma Calorimeter), ami az NA49 kísérlet detektor-együttesének egy új komponense. Az NA49 kísérlet a CERN-beli SPS (Super Proton Synchrotron) gyorsítónál üzemel.

A CMS detektor-együttes elrendezése ütköző nyalábos. Három fő tervezett alkalmazási alkalmazási területe van.

1. A Higgs-bozon(ok) keresése a $0.08 - 1 \text{TeV}$ tömegtartományban (elméleti meggondolások alapján úgy tartják, hogy a Higgs-bozon(ok) tömege ebben a tartományban valószínűsíthető).

2. Szuperszimmetrikus elméletek által jósolt részecskék keresése.

3. Nehézion-fizikai mérések (kvark-gluon plazma kísérletek).

Bármelyik alkalmazást is vesszük, a HF kaloriméternek igen fontos szerep jut, ami a detektor elhelyezéséből és geometriájából következik. A detektor két diszjunkt hengerből áll, amelyek tengelye közös a nyalábtengellyel. A két henger a CMS együttes legvégein található: $+10.860\text{m}$ és -10.860m távolságra az ütközési ponttól. A HF hengerek aktív részének sugara kicsi (1.300m) az ütközési ponttól való távolsághoz viszonyítva, így a lefedett szögtartomány is kicsi ($0 - 0.13\text{rad}$). Ebből következik, hogy a HF kaloriméter alapvetően két célra használható.

1. Egy nyers triggerjel generálására, mivel kinematikai okokból a részecskék illetve jetek többnyire kis szórási szög alatt lépnek ki az ütközési pontból.

2. A HF kaloriméter az energiamérések hermeticitásáért is felel. Mivel kis szórási szög alatt található, ezért a nagy pszeudorapiditások tartományát fedi le.

A HF kaloriméter egy kvarcszálas Cserenkov detektor. Ez egy új technika a nagyenergiás részecskefizikában. A beérkező részecskék illetve jetek részecskezáporokká alakulnak a detektor acél testében. Az acélból készült testet kvarc optikai szálak rendszere járja át, amelyek párhuzamosan futnak a HF hengerek tengelyével. A részecskezáporok nagyenergiás töltött részecskéi Cserenkov-fényt keltenek az optikai szálakban, amelyek a jelet fényelektromos sokszorozókhoz vezetik. Ezzel a beérkező részecske illetve jet energiája megmérhető.

A detektor két ok miatt kvarcszálas alapú. Egyrészt gyors válaszú berendezésre volt szükség, és a Cserenkov-jel igen gyors lefutású (a jel teljes szélessége kb 20ns), ellentétben a szcintillációs jelekkel, amelyek lassabban alakulnak ki és lassabban csengenek le. Másrészt a kvarc kitűnően bírja a sugárterhelést, kevésbé veszti el az optikai áteresztőképességét erős rádió-aktivitás esetén is, ellentétben pl az ólomüveggel. (A detektor teste különösen alacsony kobalttartalmú acélból készült, hogy a test felaktiválódását minimalizálják. Ennek ellenére, a detektortest jelentős aktiválódására lehet számítani, mivel a HF kalorimétert érő hadron fluxus kb megegyezik a CMS összes többi irányába szórt hadronok fluxusával.)

A detektor válasznak lineárisnak kell lennie az energia függvényében. Továbbá, a kalibrált detektor válaszának térben homogénnek kell lennie. A

kaloriméter felépítése miatt ez utóbbi követelmény teljesülése nem triviális. Mindkét henger ugyanis kb 216000 kvarcszálat tartalmaz, amelyek legyártása hosszú időt vett igénybe, és a gyártási periódus különböző szakaszaiban készült kvarcszálak optikai minősége fluktuálhatott. Ezért 2003 júniusaugusztusban linearitás- és homogenitásvizsgálatot végeztünk a HF kaloriméter egyik hengerének két hengercikkén. (Ezek a hengercikkek azért lettek kiválasztva, mert ezek elsőként készültek, így várhatóan ezek a legrosszabb minőségűek.) A mérésekhez az SPS gyorsító elektron és pion nyalábjait használtuk.

A dolgozat első fele HF kaloriméterrel végzett teszt-mérések ismertetését, illetve az eredmények kiértékelését tartalmazza, a következő szerkezeti vázlat szerint.

1. Áttekintés a HF kaloriméterről.

2. A teszt-méréshez használt elrendezés.

3. Kalibráció elektromágneses részecskékhez, 100GeV-es elektron nyalábbal.

4. Kalibráció hadronikus részecskékhez, 250GeV-es pion nyalábbal. Az elektromágneses illetve hadronikus részecskék jeleinek megkülönböztetése; extrapoláció 1TeV energiára. Eredmény: hadronikus/elektromágneses diszkrimináció 1TeV-en kb 4.3% bizonytalansággal végezhető.

5. Linearitás tesztek pion nyalábbal. Eredmény: alacsony energiákon a linearitás romlik.

6. Homogenitás teszt elektron nyalábbal. Eredmény: a homogenitásbeli fluktuáció 10%-kal majorálható.

Az NA49 kísérlet elrendezése fix céltárgyas. A kísérletbe újonnan beépített LGC komponensnek két alapvető szerepe van.

1. Kiegészítő detektorként a Ring Calorimeter nevű komponens akceptanciáját növeli.

2. Egy triggerjel generálására alkalmas, amely kiválasztja azon eseményeket, amelyekben nagy transzverzális impulzusú π^0 részecskék keletkeznek.

Az LGC egy ólomüveg Cserenkov detektor. Aktív térfogata 192 darab 95mm × 95mm × 680mm ólomüveg blokkból áll. A blokkok egy 12 × 16-os téglalap alakzatban vannak elhelyezve, ahol a 95mm × 95mm méretű lapok a céltárgy irányába néznek. A beérkező részecskék részecskezáporokká alakulnak az ólomüveg testekben. A nagyenergiás töltött zápor részecskék Cserenkov-fényt keltenek az ólomüvegben. Mindegyik blokkot egy-egy fototrióda olvassa ki. A detektor blokkok az OPAL kísérlet Endcap részéből származnak. (Az OPAL kísérlet a LEP –Large Electron Positron collider–gyorsítónál üzemelt, a CERN-ben.) A kiolvasórendszer alacsonyszintű része az eredeti reprodukciója.

Az LGC csak elektromágneses részecskékhez használható kaloriméterként, mivel a detektor mélysége felöleli az elektromágneses záporok teljes hosszát, ellenben a hadronikus záporok hosszának csak mintegy 30%-át.

A detektor 17.77m távolságra van a céltárgytól, előreszórási irányban, 0.13rad szög alatt a nyalábtengelytől. A téglatest alakú detektor alapéle nagyjából érinti a céltárgyból rajzolt 17.77m sugarú kört.

Ez a detektorkomponens új: beépítésére és első üzembe helyezésére 2003 októberében került sor. A dolgozat második felében a detektor első mérési

periódusának alapvető eredményeit mutatom be, a következő szerkezeti vázlat szerint.

1. Áttekintés az LGC detektorról.

2. Az LGC csatornáinak relatív kalibrációja, kozmikus sugárzás segítségével, kihasználva kozmikus sugárzás fluxusának homogenitását.

3. A $\pi^0 \rightarrow \gamma\gamma$ bomlás kinematikája: Monte Carlo becslések várható π^0 hozamra, régebbi π^+ és π^- TPC-nyom adatokból. Eredmény: az eredeti triggerrendszerrel felvett események közt az olyan események hányada, amelyek esetében az LGC-t keresztező összes detektálható részecske pontosan egy π^0 bomlásból származó fotonpárból áll, 6%-nak jósolható. A detektálható π^0 részecskék átlagos energiájára a jóslat 9.8GeV.

4. Felvett események kétfoton-tömegspektruma. Eredmény: a π^0 tömegcsúcs az LGC-vel, összehasonlítás a Monte Carlo számolásból kapott π^0 csúccsal.

1 Introduction

In this paper, studies on two calorimetric detectors from CERN experiments are summarized. The first detector is the HF (Hadronic Forward) calorimeter of CMS (Compact Muon Solenoid) complex, which is going to be used in various particle physics experiments at the accelerator LHC (Large Hadronic Collider), which is being built up at CERN. The second detector is the LGC (Lead glass Gamma Calorimeter), which is a new component of the detector complex of the experiment NA49, located at the accelerator SPS (Super Proton Synchrotron), operating at CERN.

Three main applications of the detector complex of CMS are planned.

1. Search for the presence of the Higgs boson(s) in the mass range $0.08 - 1\text{TeV}$ (which is considered to be the most likely mass range for the Higgs boson mass to be contained in).

2. Search for particles, which are predicted by SUSY (SUper SYmmetric) theories.

3. Researches in heavy-ion physics (quark-gluon plasma experiments).

In all the three applications, HF calorimeter has a crucial role, which follows from the placing and geometry of the calorimeter. The detector consists of two disjoint cylinders, both placed coaxially to the nominal beam line, at the very ends ($+10.860$m and -10.860m from the collision center) of the CMS complex. The radius of the active volume of each cylinder is small (1.300m) compared to the distance from the nominal collision center, thus the covered scattering angle range is also small ($0 - 0.13$rad). Therefore, it follows that HF can be used for two basic purposes.

1. It can serve a raw trigger signal, as due to kinematic reasons, particles or jets tend to come out at low scattering angles.

2. It provides the hermeticity of energy measurements. As it is placed at the very end (under small scattering angle), it covers the region of high pseudorapidity.

The HF calorimeter is a quartz fiber Čerenkov detector, which is a new technique in high-energy particle physics (see [2]). The the incoming particles or jets convert into particle showers in the steel body of the calorimeter. The steel body of the calorimeter is pierced by a system of quartz optical fibers (which are parallel to the nominal beam line), and the charged shower particles generate Čerenkov light signal in them. The Čerenkov signals are measured by photo multipliers. Therefore, the energy of the incoming particle or jet can be measured by the detector.

There are two main reasons for using quartz-fiber calorimetry in the very-forward region of CMS. First of all, fast response is needed, and the Čerenkov signal is very fast[1], compared to scintillators, the signal of which form and decay slower. Secondly, the quartz endures high level of radioactivity quite well: the optical aging of quartz is much slower than e.g. of lead glass, in high radioactivity environment. (The body of the detector is manufactured of steel with specially low cobalt contamination, to minimize the radioactivity, picked up by the body. However, a high level of radioactivity is expected, as the hadronic flux, covered by HF calorimeter, approximately equals to the hadronic flux in the complementer region of scattering angles.)

---

[1]The total width of the signal is about 20ns.

The detector response has to be linear in energy. Furthermore, the response of the calibrated calorimeter has to be homogeneous in space. Due to the architecture of HF[2], homogeneity test is recommended, as the optical transfers of those fibers, which were manufactured in different times, could differ. Therefore, in June-August 2003, a surface scan and linearity test was made on two sectors of HF[3], with a test beam setup at SPS. The results concerning these tests are presented in the first part of this paper.

The experiment NA49 is a fixed target experiment. The newly constructed LGC component of the experiment has two aims.

1. As an auxiliary electromagnetic calorimeter, it should increase the acceptance of the so called Ring Calorimeter component.

2. It should provide a trigger signal for selecting events, involving π^0 particles with high transversal momentum, to increase the ratio of valuable events among the total detected events.

The LGC is a lead glass Čerenkov detector. The active volume of the detector consists of 192 lead glass blocks of size 95mm × 95mm × 680mm. The blocks are placed in a 12×16 rectangle, where the faces of 95mm × 95mm size look in the direction of the target. The incoming particles convert into particle showers in the lead glass blocks. The charged shower particles generate Čerenkov light signal in the lead glass. Each block is read out by a photo triode. The lead glass Čerenkov detector blocks originate from the Endcap component of the OPAL experiment (see [3]), which was operating at the LEP accelerator (Large Electron Positron collider), at CERN. The front-end readout system is a reproduction of the original system (see [1]). The LGC is a calorimetric detector only for electromagnetic particles, as the longitudinal containment for electromagnetic showers is 100%, but the longitudinal containment for hadronic showers is about 30%.

The detector is placed at a distance of 17.77m downstream the target, under an inclination of 0.13rad from the beam line. The base of the rectangle shaped body of the detector is approximately tangential to the circle drawn from the target with a radius of 17.77m.

This detector component is quite new: the construction and first operation of the detector was in October 2003. The basic results from the first operation is summarized in the second part of this paper. These results culminate in the π^0 mass peak, which is the first physical effect, measured with the LGC.

---

[2]Both HF cylinders have about 216000 quartz fiber shower samplers.

[3]These two sectors were selected for measurements, because they were considered to be the worst in quality.

2 Test runs with HF calorimeter sectors

2.1 The HF calorimeter

An overview on the placement of HF calorimeter within the CMS detector complex can be viewed in *figure 1*.
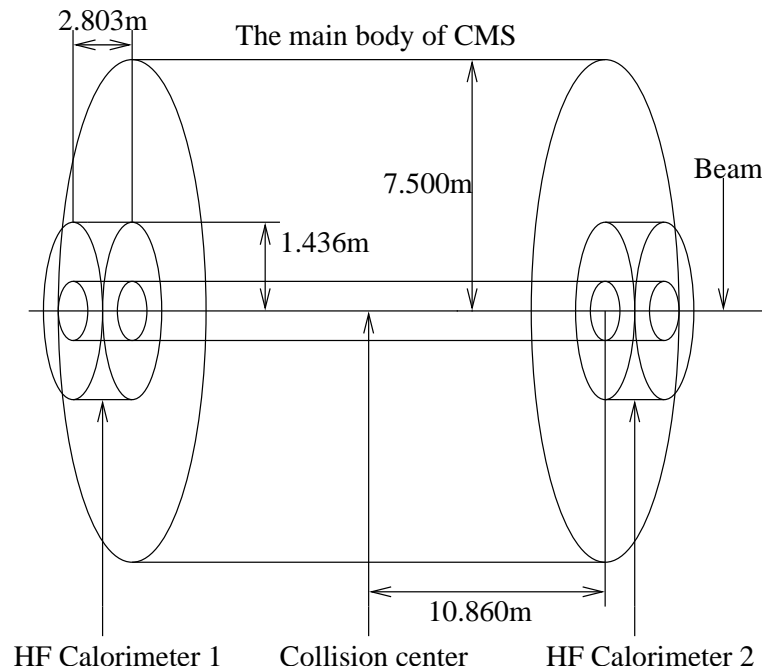

Figure 1: Sketch of the placement of HF calorimeter within CMS

It can be seen, that the HF calorimeter consists of two disjoint cylinders at the very ends of the main body of CMS. Each cylinder is built up of 18 sectors, each sector covering an angle of 20°. The sectors are called *wedges* in the HF terminology.

The wedges of the calorimeter are subdivided into 24 lower components, which are called *towers*. The tower structure of wedges are shown in *figure 2*. The towers are held together to form a wedge with steel bands, welded on the surface of the wedge.

The towers are manufactured of steel layers of thickness 5mm, by using so called diffusion (pressure) welding. If one looks at a wedge in the way as shown in *figure 2*, the steel layers in the towers are either horizontal or vertical, depending on the given tower.

Each steel layer was manufactured in such a way, to have channels on them, as shown in *figure 3*. When, as in the figure, the steel layers are attached together to form a tower, the channels pierce the steel body as a uniform grid like system of pipe holes, where the pipe holes are parallel to the axis of the given HF cylinder.

The channels are used to insert quartz optical fibers of diameter 0.8mm in them[4], which were specially manufactured for this detector. When a high-energetic charged shower particle crosses a fiber, Čerenkov light is produced, and the light is guided to a photo multiplier on one end of the fiber. Each tower has one special channel in it: it does not contain an optical fiber,

---

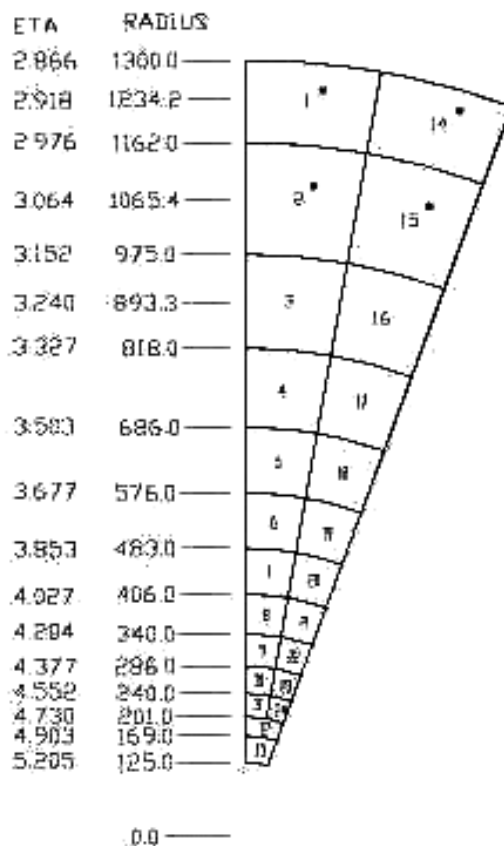[4]The quartz core is 0.6mm in diameter, with 0.1mm plastic coating.

10

Figure 2: The tower structure of a wedge

it is used to insert an isotope wire in it for test purposes and for on-line monitoring of the aging of fibers.

The quartz fibers are read out in such a way, that they are collected into certain groups, and led to photo multipliers. The photo multipliers and the readout electronics are placed in a so called *readout box* on that end of the given wedge of a HF cylinder, which does not face the direct rays from the collision center. The readout boxes are protected by lead shields to minimize the radiation damage.

There are two kinds of fiber length types. The default fiber length covers the full length of the steel cylinder (these are called electromagnetic fibers). Every second fiber ends 22cm earlier on that end of the cylinder, which faces the collision center (these are called hadronic fibers). The length difference between the two fiber types is used to distinguish the hadronic particles or jets from the electromagnetic particles or jets, as the hadronic showers develop much deeper in the steel body of the detector than the electromagnetic showers. This length difference is controlled by steel wires, which are inserted into each hadronic channel to push the hadronic fibers back by 22cm.

In every tower, both the electromagnetic fibers and the hadronic fibers are collected separately, and are led to photo multipliers; one for the electromagnetic fibers, one for the hadronic fibers. Thus, a wedge has 2×24 photo multipliers. For simplicity, the complex of electromagnetic fibers of a given tower, or the complex of hadronic fibers of a given tower, will be referred

11

A single steel layer

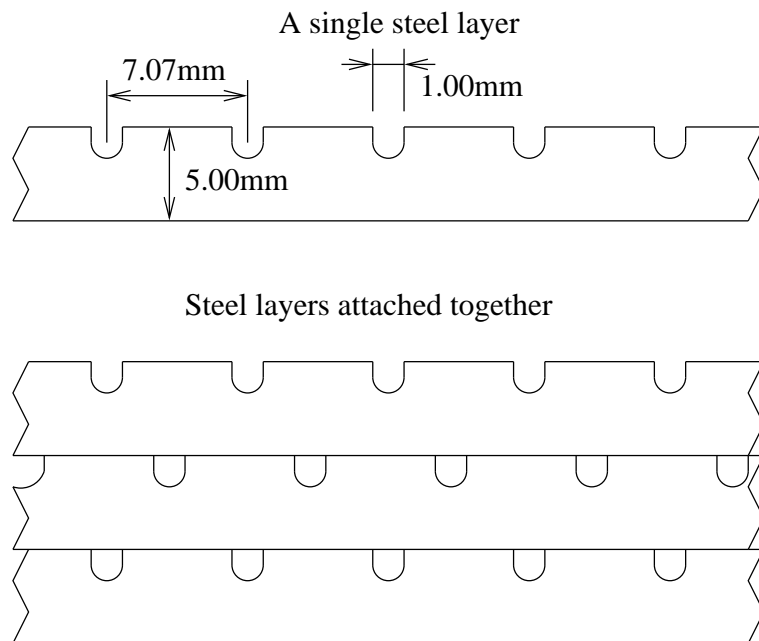7.07mm   1.00mm

5.00mm

Steel layers attached together

Figure 3: Channel structure on the steel layers

as simply a given *electromagnetic tower* or a given *hadronic tower*, respectively. Note, that each electromagnetic tower geometrically contains precisely one hadronic tower.

There are 5 test fibers for each photo multiplier, which are collected together, and can be pulsed with a ultra violet nitrogen laser signal, to monitor the aging of the photo multipliers on-line.

Figure 4 shows the mounting process of a HF cylinder. The end with readout boxes can be seen in the right side of the cylinder.

Each wedge contains about 12000 quartz fibers: about 6000 electromagnetic and about 6000 hadronic fibers. These were manufactured in a quite long period of time, and it was not certain, that the homogeneity of energy response is guaranteed (that is, it was not sure, that the optical transfer quality of the fibers are the same). Therefore, test runs were made with two of the HF wedges[5] in June-August 2003 at the SPS accelerator of CERN, to perform surface scan for homogeneity test. Furthermore, a linearity test in energy was also carried out.

---

[5]These wedges were the earliest ones, thus they were supposed to be the worst in quality.
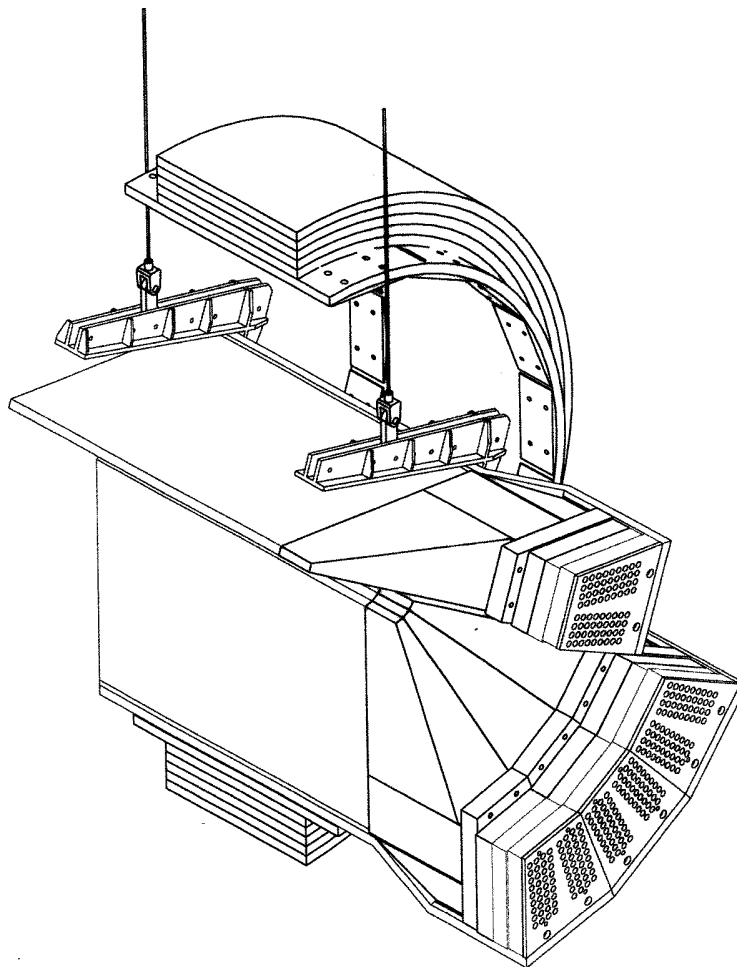
Figure 4: The mounting of a HF cylinder

2.2 Test run setup

The test runs for surface scan was performed with defocused 100GeV e^- beam, and with defocused 250GeV π^- beam. Linearity tests were carried out with defocused π^- beams of $30, 50, 100, 150, 200, 300$GeV in energy. The sketch of setup can be seen in *figure 5*.

Two wedges were placed on a moving table, they were identified by the labels *left* and *right*, which originate from the geometrical placing on the test table. There was a shift and a lift device under the table, so the impact point of the nominal beam line could be moved to arbitrary points of the front surface of wedges. The table coordinates were read automatically by the DAQ, with a precision of 0.1mm.

When the wedges will be operating in the CMS experiment, particles or jets, coming from the collision center, are going to reach the face points of HF calorimeter under certain inclinations, relative to the nominal beam line. In order to simulate this effect, there was also a tilt device mounted on the test table. By tilting the wedges at appropriate angles, one could simulate that the beam particles are particles arriving from the CMS collision center. The tilt coordinates were also read automatically by the DAQ, with a precision of 0.1mm.

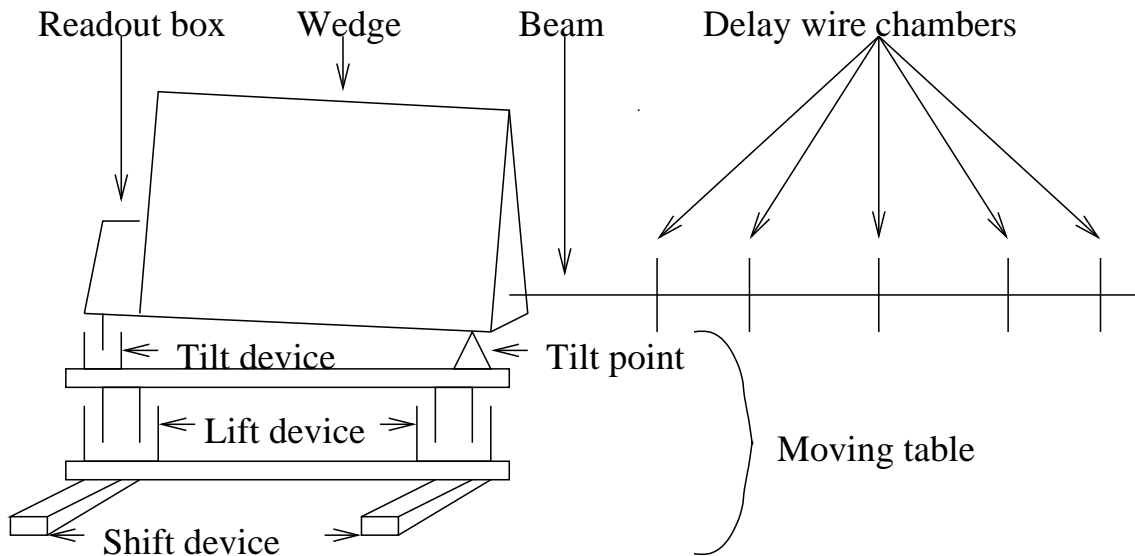Due to the defocusing of the beam, the particles reached the wedge surface in a circle of

Figure 5: The testbeam setup

5cm in diameter, at every table position. The incident particles could be tracked with the 5 delay wire chambers in front of the test table, by fitting straight line on the delay wire chamber data. Thus, by knowing the table and tilt coordinates, and the delay wire chamber data for every incident particle, it was possible to reconstruct the impact points with an error of 0.1mm. Therefore, by moving the table according to a certain coordinate grid (the scale of which is about 3cm), one can make a radioscopy of a whole wedge front surface for a calibrated wedge.

The table and tilt coordinates were read out at every 100ms by the so called slow DAQ. For the physical DAQ, a fast readout system was used: when the trigger signal (which was generated by upstream scintillators) arrived, the delay wire chamber coordinates were read out; furthermore the analog-digital converted signals of HF photo multipliers were recorded with 25ns time-binning, for 20 time-bins. The photo multiplier signals were delayed by at least 4 time-bins, therefore the pedestal values of the analog-digital converters could be obtained event-by-event, as there was always zero signal in the first 3 time-bins. A typical raw signal of a tower for a particle impact, recorded by the DAQ, is shown in *figure 6*. The ADC equivalent of charge measured by a photo multiplier (which is called the *charge* in the HF terminology), is defined by the value of $(sig[max-1]+sig[max]+sig[max+1]+sig[max+2])-\frac{4}{3}(sig[0]+sig[1]+sig[2])$, where the recorded ADC values in the time bins are ordered in the array $sig[0\ldots19]$, and max is the array entry with the maximum signal value. The delay of analog signals was arranged in such a way, that $max \geq 4$ was always valid for correctly recorded events. In this paper, we will also use the terminus *response* for the notion of *charge*.
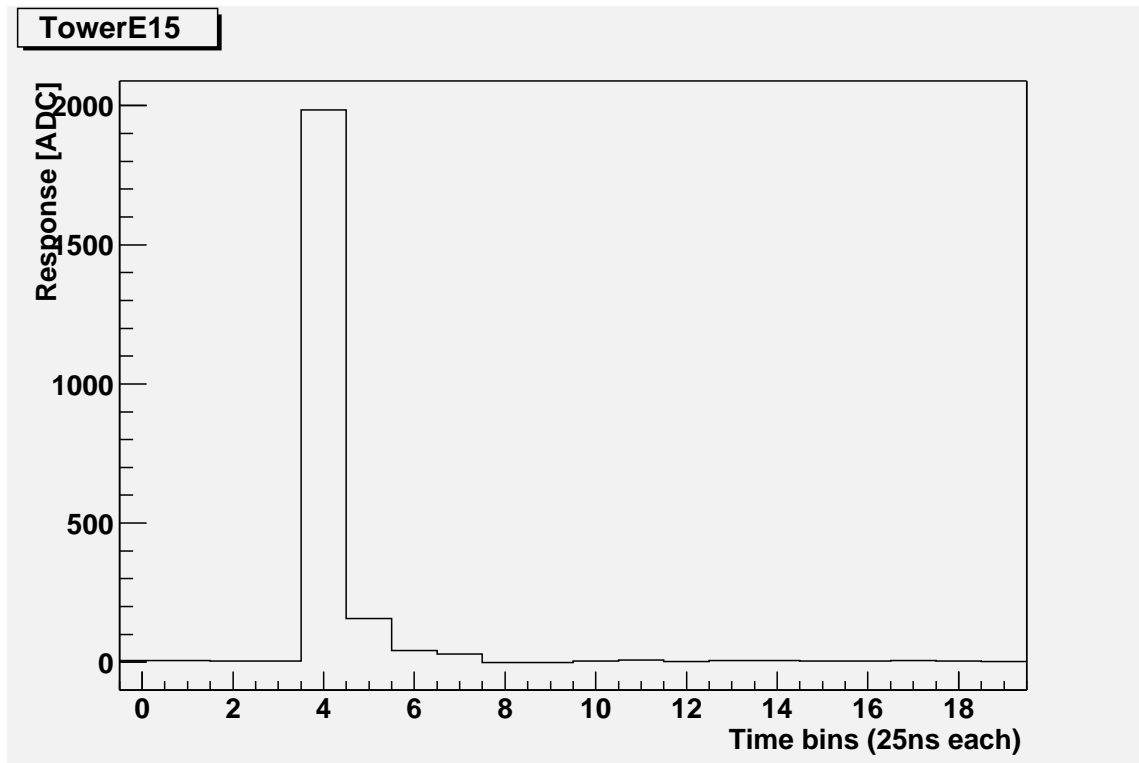
Figure 6: Typical raw signal

2.3 Calibration

2.3.1 Calibration of the electromagnetic towers by 100GeV e^- beam

The calibration of the towers are best done using focused beam. There were no focused beam data taken, therefore the calibration factors of the electromagnetic towers were obtained by simulating focused beam data from defocused, in the following way. Certain small domains (let us call them *simulated focused beam shot-points*) were defined on the wedge surface, one in each tower, in such a way that the electromagnetic shower leakage (from the wedge to the air) should be negligible, if electromagnetic particles were shot into those areas.

By using the whole database of the electron surface scan, electromagnetic tower responses for such particles, which arrived into a given tower's simulated focused beam shot-point, were averaged. This process was performed for every tower, thus a matrix of average electromagnetic responses was obtained, where the rows indicate successively the towers where the simulated focused beam was directed, and the columns indicate all the towers successively. The number of the nonzero elements in every row was reduced by forcing the average electromagnetic response of those towers to be zero, which are not the neighbors of the tower, where the simulated focused beam was directed.

After this process, one has a system of equations: the previous matrix acting on the column-vector of the (unknown) electromagnetic tower gains, one gets a column-vector containing constant 100GeV. By solving this system of equations (that is, by inverting the matrix) the electromagnetic tower gains were obtained.

The same process can be carried out to obtain the calibration factors of the electromagnetic

towers, with 250GeV π^- beam.[6]

After the above process, the electromagnetic towers were calibrated either for electromagnetic, or for hadronic particles.

2.3.2 Relative calibration of hadronic and electromagnetic towers by 250GeV π^- beam

The relative calibration of hadronic/electromagnetic part of each tower was done by using the fact that for every tower, the hadronic fiber system (hadronic tower) is geometrically contained by the electromagnetic fiber system (electromagnetic tower). Thus for every tower, the energy deposition in the hadronic region is bounded by the energy deposition in the electromagnetic region. This fact does not depend on the type (i.e. hadronic or electromagnetic) of the incident particle.

Assuming that the hadronic and electromagnetic part of a given tower is absolutely calibrated (for a given type of particles), one can take the histogram of the ratio of hadronic and electromagnetic tower response (for the given type of particles). The electromagnetic showers tend to deposit most of their energy in the first 22cm of the electromagnetic tower, the hadronic showers (as they are develop much deeper in matter) tend to deposit most of their energy in the hadronic tower, after the first 22cm of electromagnetic tower. Therefore, the introduced ratio tends to be 1 for hadronic particles, and tends to be much lower than 1 for electromagnetic particles. Thus, in both cases there is going to be a peak in the introduced histogram: in the case of hadronic particles, the position of the peak is at 1, and in the case of electromagnetic particles, the position of the peak is much lower than 1. Furthermore, there is going to be a sudden cutoff in the histogram at 1 in the case of hadronic particles, because the energy deposited in the hadronic tower cannot exceed the energy deposited in the electromagnetic tower.

The above argument can be reverted in order to solve for the relative calibration of the hadronic/electromagnetic towers. If the hadronic/electromagnetic relative calibration factor is unknown, but the histogram of hadronic/electromagnetic tower response for hadronic (e.g. π^-) particles is recorded, one can assign the inverse of the hadronic/electromagnetic relative calibration factor to the place of the peak in the histogram. An advantage of this method is, that it is not sensitive for shower leakage.

One can see a demonstration of the above process for tower 1 of left wedge in *figure 7, 8*. As the resolution of the HF calorimeter is not really good at the energy scale $100 - 250$GeV (the number of photo electrons, emitted by the cathode of the photo multipliers is low), the sudden cutoff at 1 for hadronic particles cannot be seen: it is masked by the spread of the distribution. For the sake of demonstration, hadronic/electromagnetic tower response ratio is corrected by the factor 1.7 in *figure 7, 8*, which was previously known to be the approximate relative calibration factor between the hadronic and electromagnetic tower of tower 1, as a thumb rule (it was known from laser-pulse runs).

Once the relative calibration of the hadronic/electromagnetic towers is measured, the above

---

[6]Hadronic particles, with a given energy, do not make the same energy response as electromagnetic particles with the same given energy. This is because the showers, developed by the two kinds of particles, differ in structure a lot. Consequently, the calibration factor for electromagnetic particles does not equal, in general, to the calibration factor for hadronic particles. (There is no thumb rule for the ratio of the two kinds of calibration factors, it depends on the calorimeter type.) Therefore, discrimination between hadronic and electromagnetic particles is necessary, in order to know which factors to use for the signals of a given particle impact.
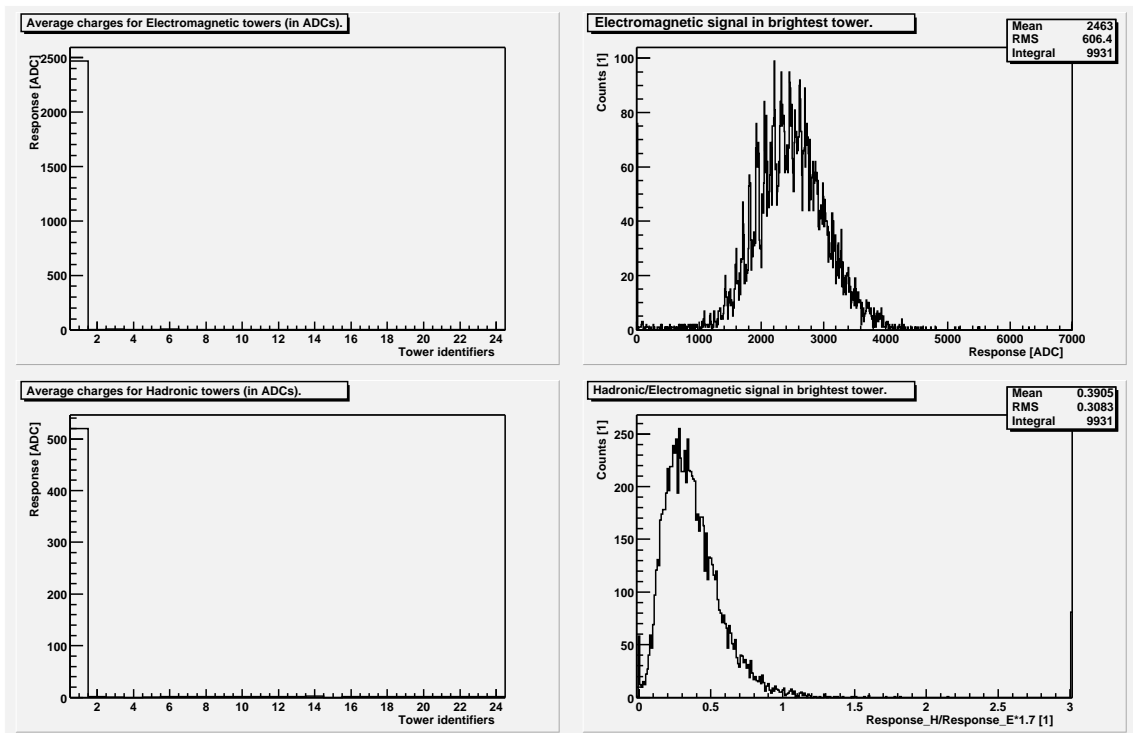
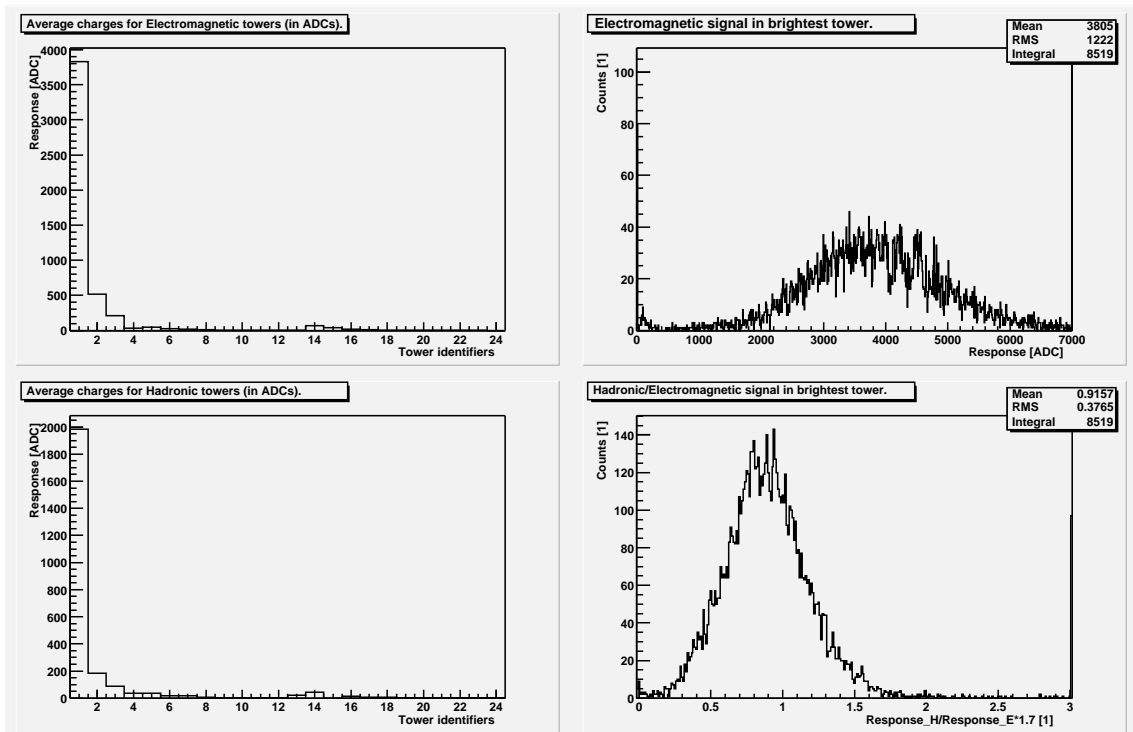Figure 7: The histogram of hadronic/electromagnetic tower signal ratio for 100GeV e^- beam

Figure 8: The histogram of hadronic/electromagnetic tower signal ratio for 250GeV π^- beam

17

argument can also be used to distinguish the signals of electromagnetic particles from the signals of hadronic particles, by measuring the hadronic/electromagnetic tower response ratio. One can make an extrapolation for 1TeV particles: the standard deviation of the distribution of hadronic/electromagnetic tower signal ratio is expected to drop down by the factor $\frac{1}{\sqrt{1\text{TeV}/100\text{GeV}}}$ in the e^- case, and by the factor $\frac{1}{\sqrt{1\text{TeV}/250\text{GeV}}}$ in the π^- case, compared to the values displayed in *figure 7, 8*. By approximating the distributions with Gaussian distribution, one has that at 1TeV, the incident particles can be distinguished with an uncertainty of approximately 4.3%.

As a summary we can state, that given an unknown incident particle, the particle type (i.e. hadronic or electromagnetic) can be determined by measuring the hadronic/electromagnetic response ratio. Knowing the particle type, one uses the appropriate (i.e. hadronic or electromagnetic) calibration factors of the electromagnetic part of the towers, thus one can obtain the energy (and type) of the incident particle.

2.4   Linearity test of energy response with π^- beam

During the testbeam period of 2003, linearity test was made on towers 2 and 17 of the left wedge. π^- beam was used. The beam energies were $30, 50, 100, 150, 200, 300 \mathrm{GeV}$. Unfortunately, the $30 \mathrm{GeV}$ point is not usable, due to possibly high e^- contamination of the beam.

Test of linearity in towers E2 and E17

Figure 9: Test of linearity of energy response for E2 and E17
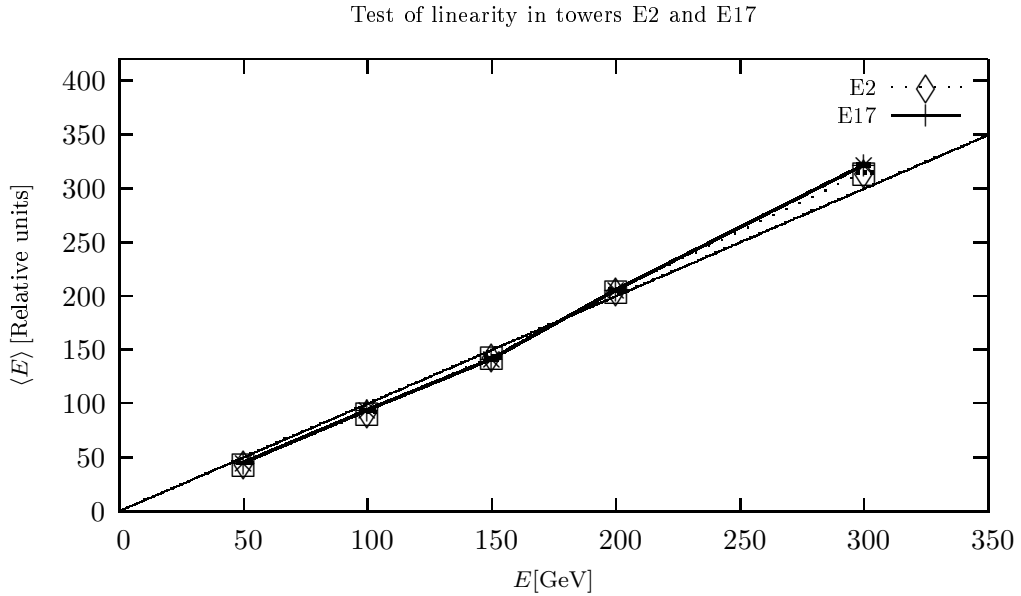
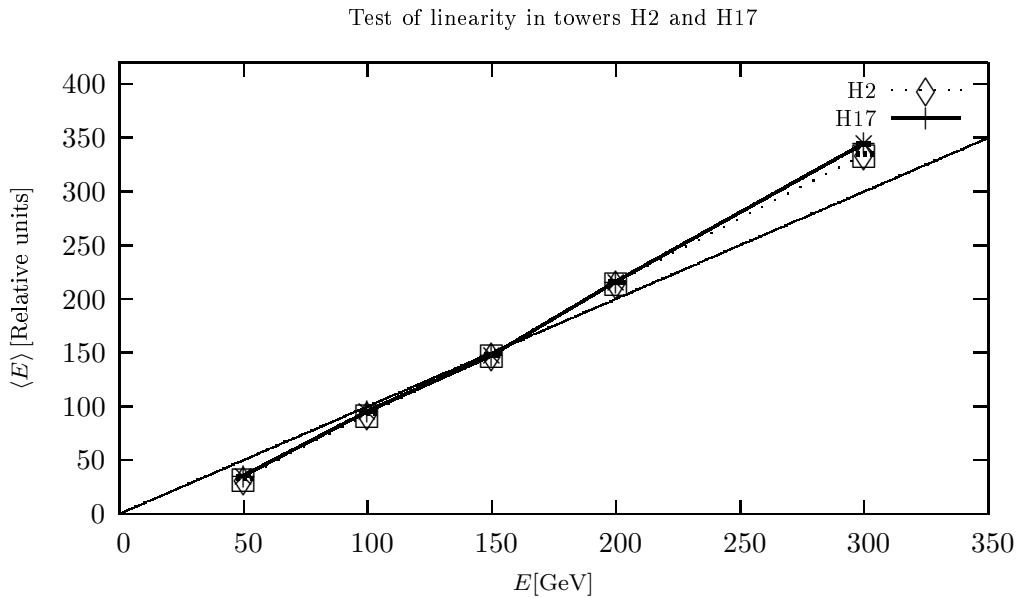Test of linearity in towers H2 and H17

Figure 10: Test of linearity of energy response for H2 and H17

The measured points and the linear fit for E2 and E17 are shown in *figure 9*, and the similar plot for H2 and H17 is shown in figure *figure 10* (by linear curve we mean a map $x \mapsto a \cdot x$ for a

19

real number a). Note, that on these plots the measured points of towers 2 and 17 are scaled into each-other in such a way, that the linear curves fitted to them correspond. The errorbars are drawn on the figures, but the statistical errors happen to be very small (all the measurement points are averages on about 50000 events), therefore the errorbars are hardly visible.

For the linearity tests of towers 2 and 17 calibration is not needed, as they are big enough to contain the hadronic showers: it turned out that for π^- particles, which reach the wedge near the center of these towers, the shower leakage is zero to the neighboring towers. Thus, taking the responses of the closest neighboring towers into account is unnecessary. Therefore, at every point of measurement, the raw energy responses (which are measured in raw ADC units) were used to calculate the average response, the standard deviation of response, and the statistical error of average response. For incoming particles with energy E, the average response is denoted by $\langle E \rangle$, and the standard deviation of response is denoted by $\sigma(E)$.

To be able to characterize the nonlinearity of the response quantitatively, we introduce a notion of linearity error, which is defined in the following way. First, linear fit is performed on the measured points. Then, the ratio of the difference from linear fit and the corresponding value of the linear fit is calculated for each point of measurement. The error of linearity is defined to be the average of these ratio values. The error of linearity proved to be about 6% for E2 and E17, while about 12% for H2 and H17.

In *figure 11*, the rule of $\frac{\sigma(E)}{\langle E \rangle} \sim \frac{1}{\sqrt{E}}$ is demonstrated for E2 and E17, and the similar plot for H2 and H17 is shown in *figure 12*. Note, that the points of towers 2 and 17 are again scaled into each-other, like in the case of linearity test.
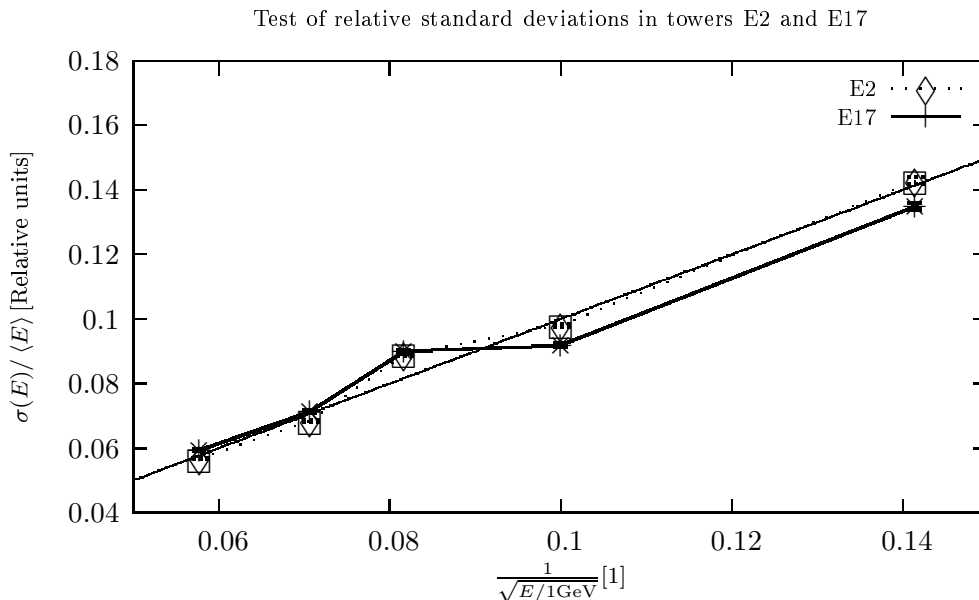

Figure 11: Energy dependence of the relative standard deviation (E2, E17)

It can be seen from the plots, that linearity is not so good at low energies, both in the case of electromagnetic and hadronic towers. As the curves of tower 2 and 17 follow each-other both in the hadronic and in the electromagnetic case, it can be stated, that this property of the detector is universal: it does not depend on the tower. Furthermore, in the hadronic case, linearity at lower energies is worse than in the electromagnetic case. This is most probably

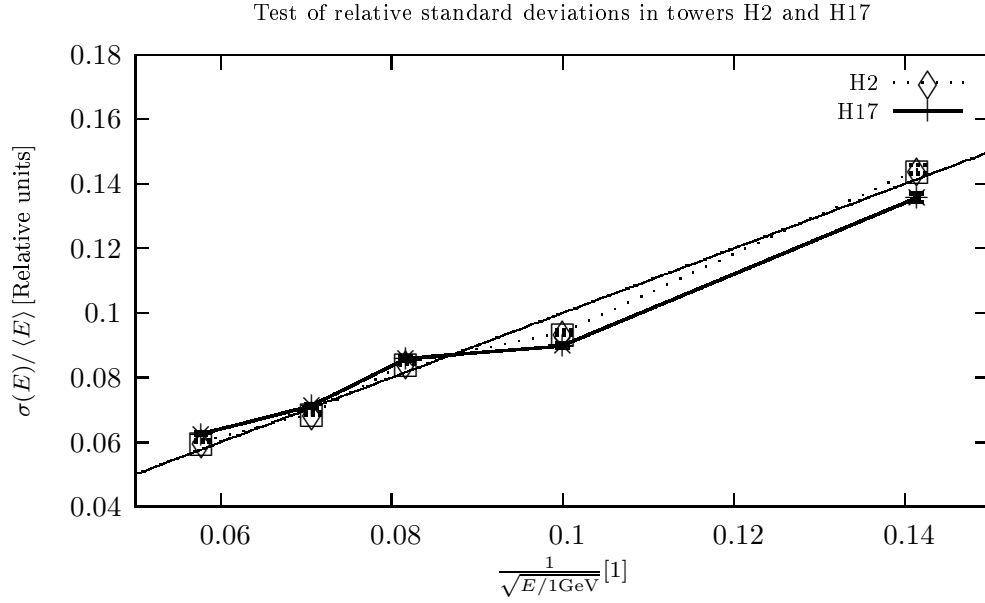Test of relative standard deviations in towers H2 and H17

Figure 12: Energy dependence of the relative standard deviation (H2, H17)

due to the fact, that hadronic showers do not develop deep enough in matter at lower energies, therefore lesser energy is deposited in the hadronic region of a given tower.

To show that linearity holds better in the high energetic region, we present *figure 13*, where the linearity plots are shown in log-log scale.
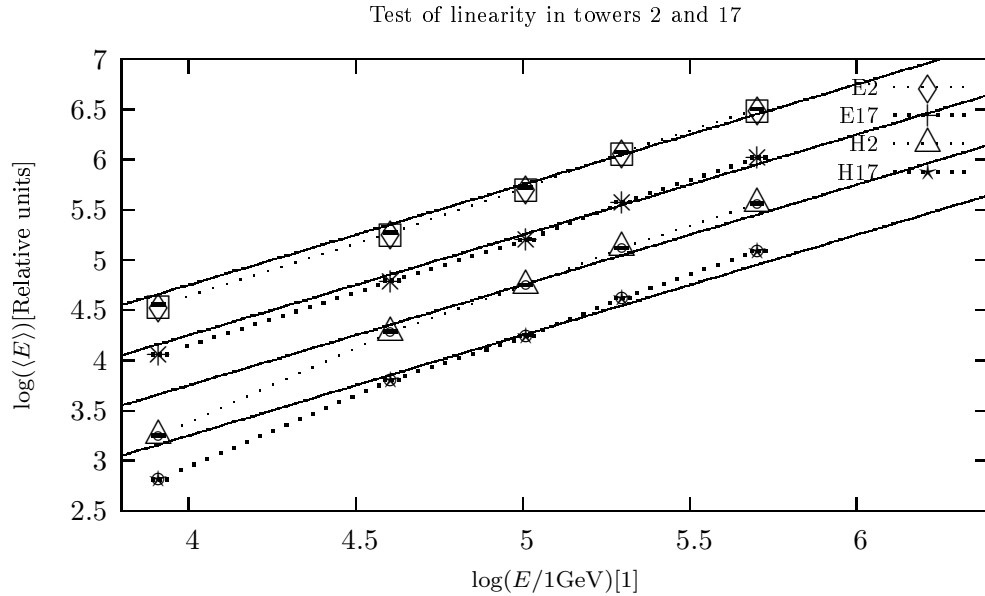
Test of linearity in towers 2 and 17

Figure 13: Test of linearity of energy response for towers 2 and 17

When a response function $E \mapsto \langle E \rangle$ is linear, then the corresponding curve is parallel to the solid lines, drawn in *figure 13*.

2.5 Surface scans for homogeneity test

The surface scans were performed by the introduced testbeam setup. Scans were made both with 100GeV e^- beam and with 250GeV π^- beam. Unfortunately, the quality of π^- beam was not really good (probably the e^- contamination was high), and was not quite stable in time. Therefore, the results of π^- scans do not have much significance.

The spatial binning, which was introduced on the front surface of the corresponding wedges in order to obtain the appropriate histograms of energy response in space, was of size 5.876mm× 4.515mm (vertical × horizontal). Here, by the vertical direction we mean the vertical direction of the testbeam setup, which corresponds to the horizontal direction of the presented plots. The bin coordinates will be indexed by a pair of numbers (x, y).

By the energy response, we mean the energy response calculated from the raw signals of electromagnetic towers, by taking the electromagnetic calibration factors into account. The similar homogeneity test for the energy response, calculated from the raw signals of hadronic towers, would only make sense in the case of π^- scans, as in the case of e^- scans showers hardly reach the region of hadronic towers.

First, we introduce three kind of histograms: the number of particle hits in bins (denoted by $(x, y) \mapsto N$), the average energy response in bins (denoted by $(x, y) \mapsto \langle E \rangle$), and the standard deviation of energy response in bins (denoted by $(x, y) \mapsto \sigma(E)$).
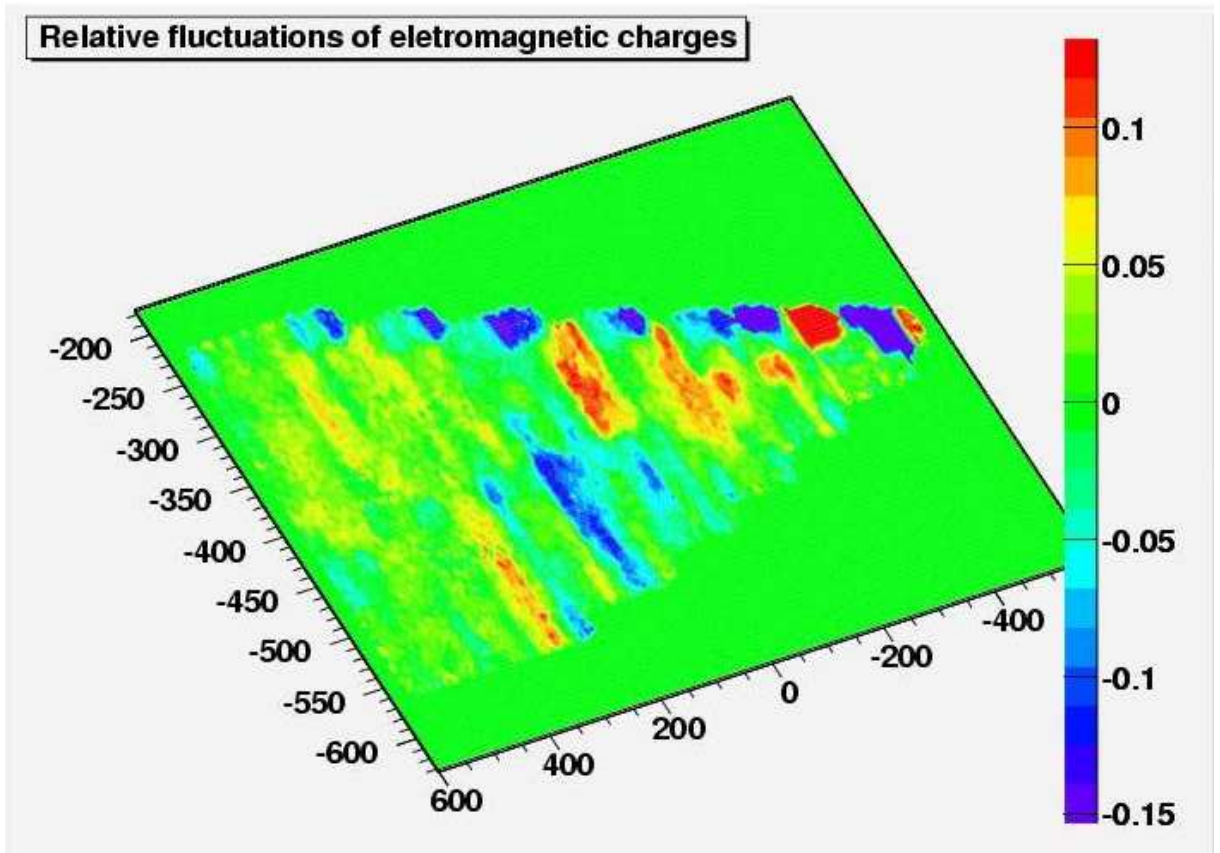

Figure 14: Relative fluctuations of electromagnetic energy response (left wedge)

By the histogram of relative fluctuations we mean the histogram $(x, y) \mapsto \frac{\langle E \rangle - \overline{E}}{\overline{E}}$, where $\overline{E}$
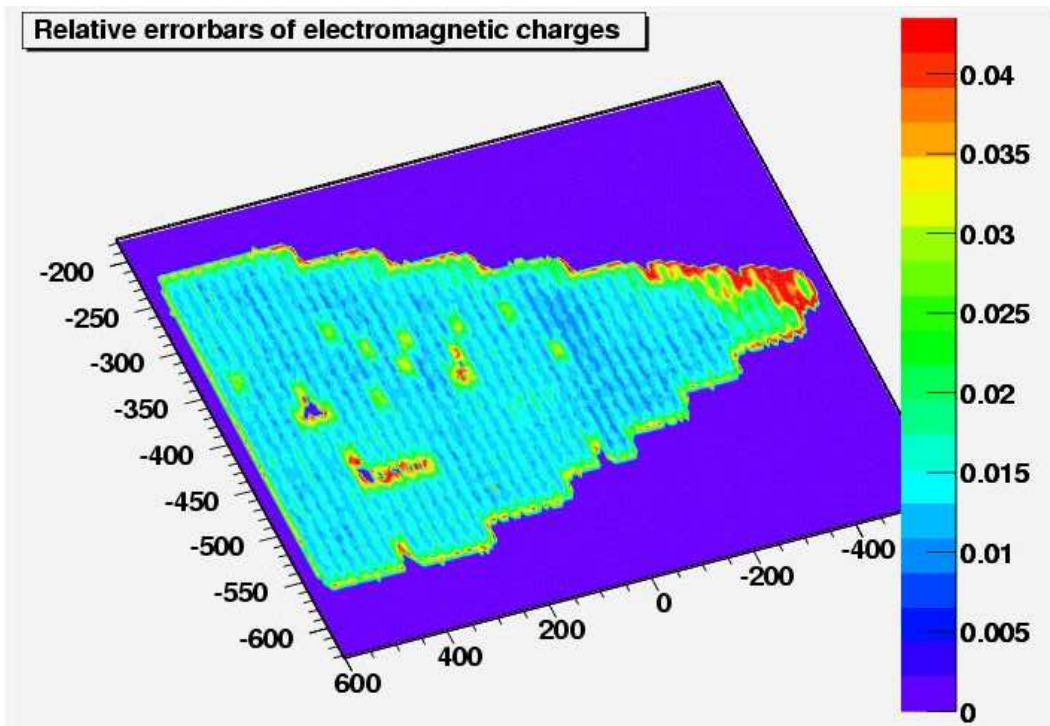
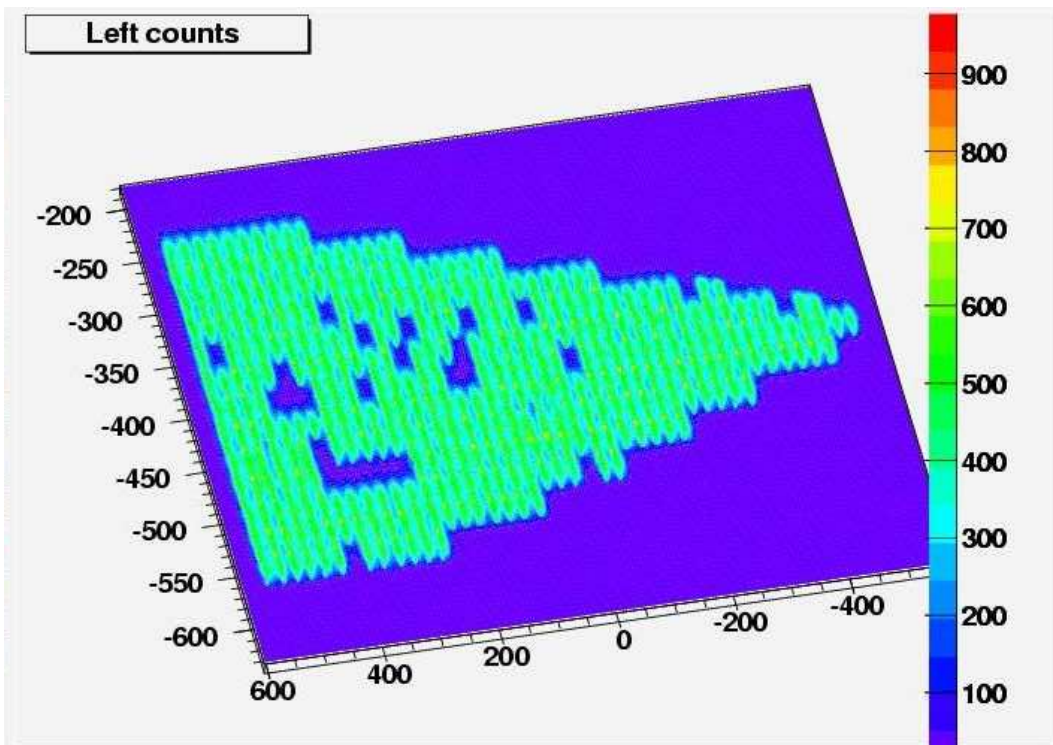Figure 15: Relative errorbars of electromagnetic responses (left wedge)

Figure 16: Particle hit counts (left wedge)

is the mean value of the histogram $(x, y) \mapsto \langle E \rangle$. The histogram of relative errorbars means the histogram $(x, y) \mapsto \frac{\sigma(E)/\sqrt{N}}{\langle E \rangle}$. The histogram of counts means $(x, y) \mapsto N$.

The result of the homogeneity tests of energy response with 100GeV e^- beam for the left wedge can be seen in *figure 14, 15, 16*. The similar result for the right wedge can be seen in *figure 17*. In both cases, the following observations hold. The relative errorbars of the energy response can be bounded by 2% on the relevant regions. The inhomogeneity of energy response can be bounded by 10%.

The impact point of a test particle was determined by the wire chamber tracking, as explained before. The energy response of a given particle impact was calculated by taking only the signals of closest neighboring towers of the impact point into account, to prevent the spreading of the signals of possibly noisy towers.
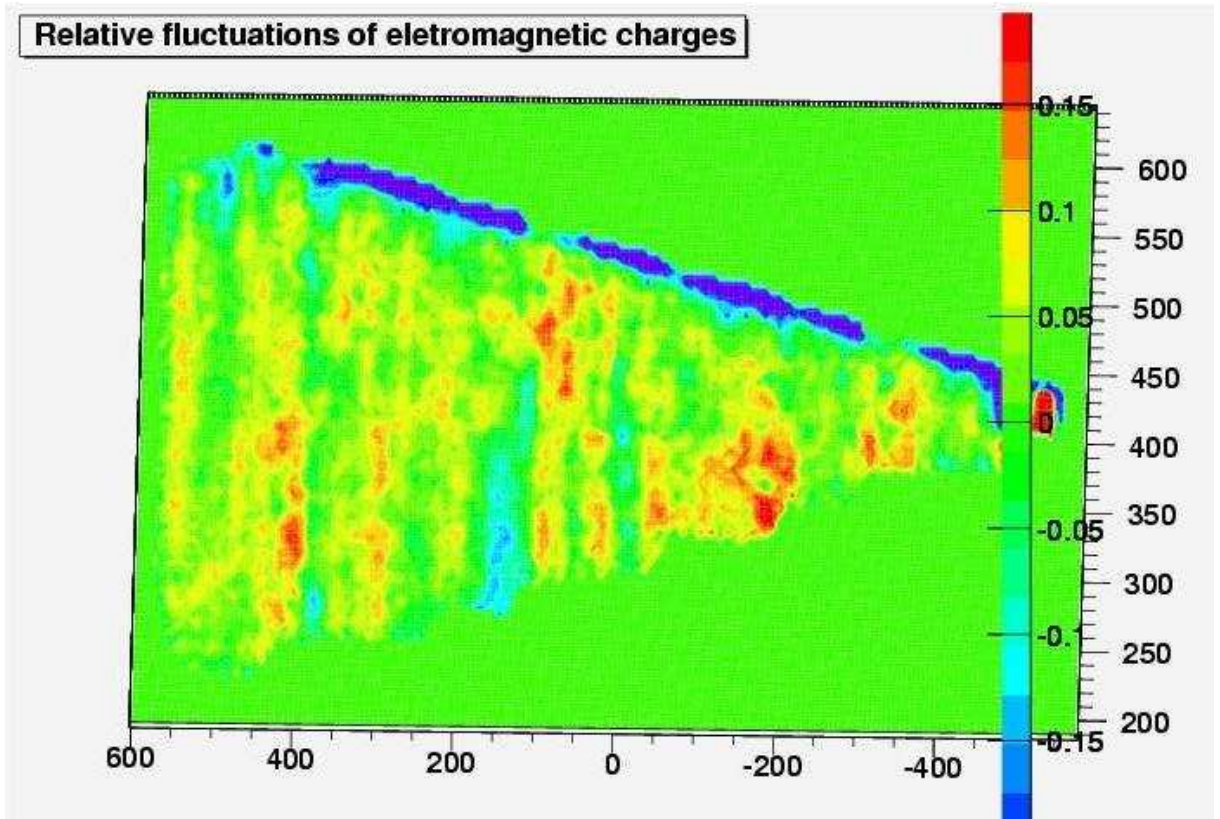

Figure 17: Relative fluctuations of electromagnetic energy response (right wedge)

One can see some empty domains in the histograms of counts: these are due to missing scan spots. A slight asymmetry can be seen in the histograms of relative flucuation of energy response, around the wedge borders. This is due to the effect of shower leakage into the air when particles arrive near the border of a wedge, and to the fact that the scan domains themselves are asymmetrically placed on the wedge surfaces. Thus, on one border, there is shower leakage, while on th other it cannot be seen.

3 The construction and first operation of the LGC detector

3.1 An overview of LGC in NA49

The experiment NA49 is a fixed target setup. The current architecture can be viewed in *figure 18*. The blue colored bar indicates the newly built LGC detector.
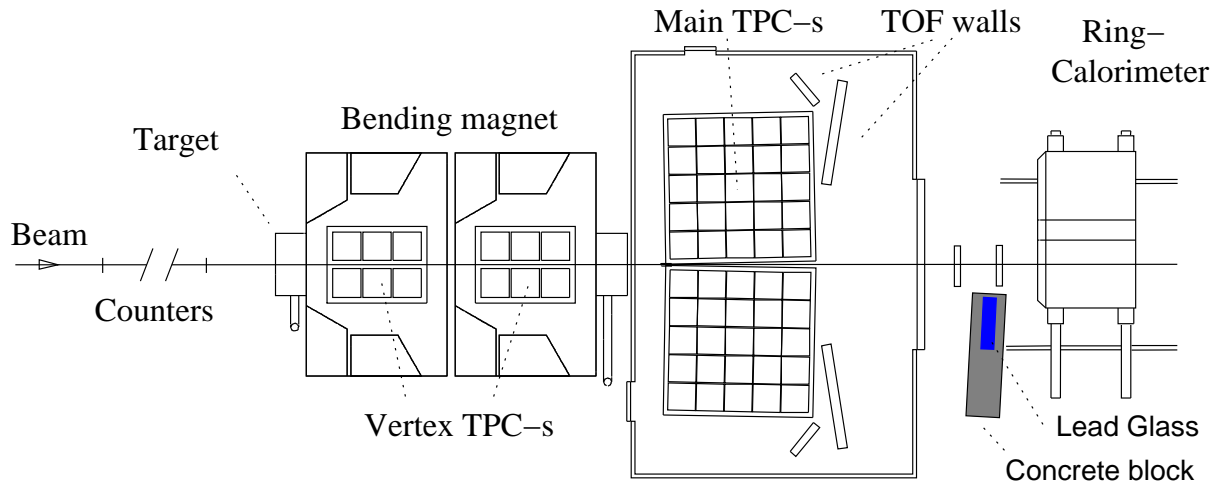

Figure 18: Sketch of the current architecture of NA49

The horizontal distance between the target and the center of the front face of LGC is measured to be 17.77m. The inclination of the front face of LGC is measured to be 0.13rad. The distance from the nominal beam line is 156cm. The inclination of the front face was chosen in such a way, that it is approximately tangential to the circle, drawn from the target with a radius of 17.77m.

The LGC is built up of lead glass Čerenkov detector blocks, which were dismounted from the Endcap component of the OPAL experiment. The lead glass detector blocks were applied as an electromagnetic calorimeter at Endcap. Each detector block contains a lead glass block of size $95\text{mm} \times 95\text{mm} \times 680\text{mm}$, which is read out by a photo triode at one of the $95\text{mm} \times 95\text{mm}$ sized faces. The blocks are placed in a 12×16 rectangle, with their $95\text{mm} \times 95\text{mm}$ sized faces (which do not carry photo triode) looking in the direction of the target (thus the photo triodes do not get direct rays from the target). Each detector block contains a small integrated amplifier to amplify the response of the photo triode, before loading the signal onto a shielded cable, which leads to the DAQ electronics, located in the counting-room, at approximately 20m cable-length from the experimental area.

The photo triodes are fed by high voltage supplies of -1000V and -500V, and a ground. The integrated amplifiers are fed by low voltage supplies of -12V, $+12\text{V}$ and 0V, which are independent of the ground. The signal from each block is loaded onto a cable of shielded twisted pair: the analog signal is reconstructed by the DAQ electronics as the difference of voltage levels on the two lines of the twisted pair. This method reduces the noise, picked up along the cable.

Two kinds of test pulse apparatus are built in each block. There is an optical fiber connection built in, for ultra violet nitrogen laser pulsers. This facility is not used by us. Furthermore, there is a LED in each block, which can be pulsed to monitor the possible amplification changing on-line. Each LED is fed by a shielded twisted pair, for the same reason as explained for the

signal cables.

The LGC detector can be viewed in *figure 19*. This is the front face; particles from the target enter here. The ends with the photo triodes, and the readout cables are on the back side, which is shown in *figure 20*.
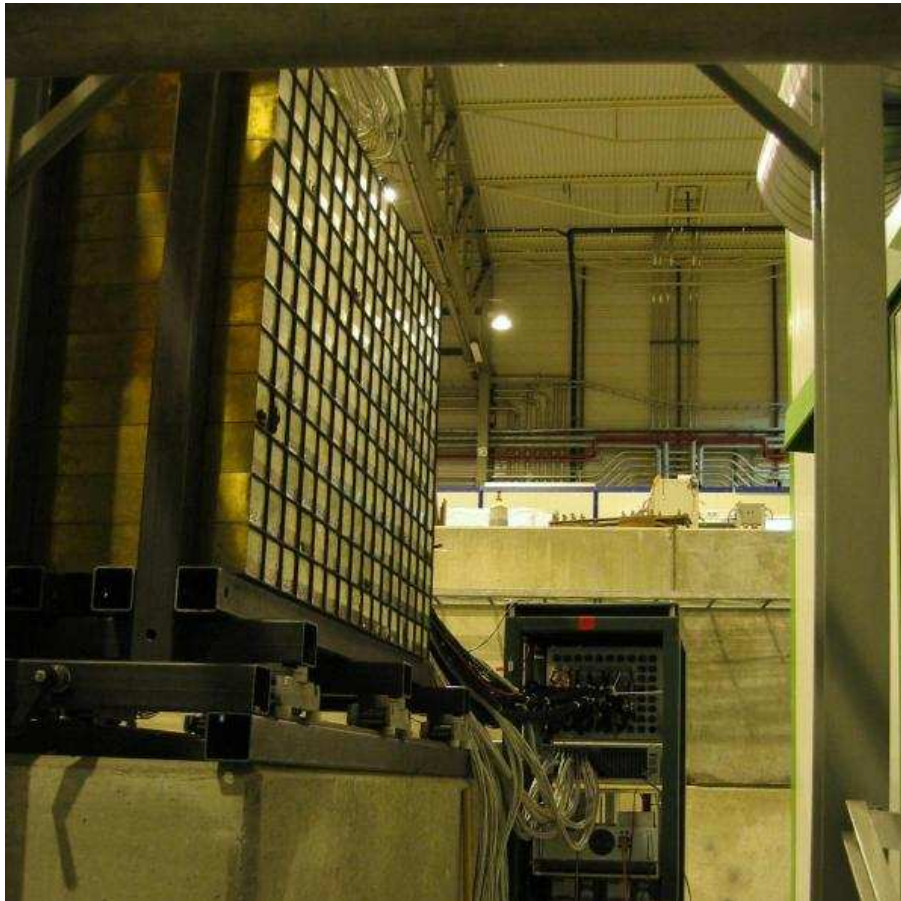

Figure 19: The front of LGC

LGC was built to catch events involving π^0 particles with high transversal momentum. The energy of a π^0 particle is measured via the $\pi^0 \rightarrow \gamma\gamma$ reaction, which covers the 99% of π^0 decays. A schematic of such a decay is shown in *figure 21*. The decay point is always located in the target, as the π^0 particles do not have enough time to propagate on mm scales, before decay. (A π^0 particle with energy 1TeV approximately would propagate 0.25mm in the laboratory system, before decay.)

By taking the coincidence of the LGC signal with the original NA49 trigger system(s), the ratio of valuable events among the total recorded events can be raised. This would be important, because the DAQ system of NA49 can store at most about 30 events per second. During the runs performed in October 2003, the so called n+p trigger system was used by default, when a trigger signal, independent from LGC, was needed. (The n+p setup is one of the original trigger systems of NA49: there are several other trigger facilities built in, apart from this.) The predicted ratio of the LGC trigger events among the total recorded events with the original n+p setup will be discussed later, as a result of a Monte Carlo simulation, based on previously recorded TPC-track data.
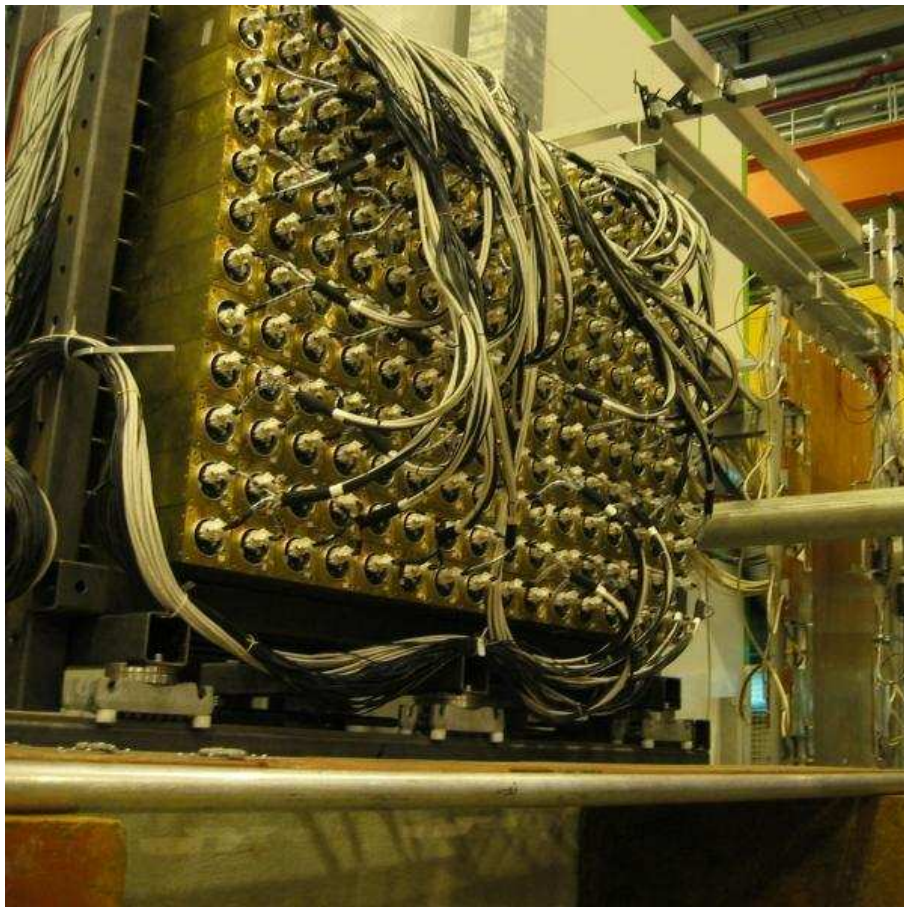
Figure 20: The back of LGC

The signal of a single block (which is called *channel* in the LGC terminology) for a real particle is shown in *figure 22*. The short 150ns NIM signal on the figure is the so called *beam trigger* signal, which is generated by two upstream scintillators (this is the raw trigger signal of NA49). As it can be seen, the LGC signal is relatively slow, but the beginning of the signal runs up fast (on 100ns scale). Therefore, the LGC signal may be applied as trigger signal.

After the LGC signal from the channels arrive at the counting-room on shielded twisted pairs, the signal is split up: one branch is led to the analog-digital converters (for energy measurements), one branch is led to the trigger unit. The trigger unit is an analog device, which multiplies the channel signals by adjustable factors, then calculates the sum of the weighted signals for every 4 neighboring channels. If the resulting signal of a 4-tuple is higher than an adjustable global threshold, then an LGC trigger signal is generated.[7] This signal is shown in *figure 23* as *Trigger*.[8]

---

[7]The summing on every 4 neighboring channel is performed, because a gamma photon need not, in general, hit the center of a channel: the total deposited energy can split up between 4 closest neighboring channels.

[8]For historical reasons, the signal labeled *Trigger* is not exactly this, in reality. Originally, two LGC calorimeters were planned to be built, both of size 12×8 channels, symmetrically placed to the nominal beam line. They would generate signals *Trigger1* and *Trigger2* as explained, and the logical *or* of them would be the signal labeled *Trigger*. Due to lack of room in the experimental area, this could not be carried out, therefore the two LGC halves are physically built together on one side of the beam, forming a single calorimeter of size 12×16 channels, but having the trigger units of two calorimeters of size 12×8 channels.
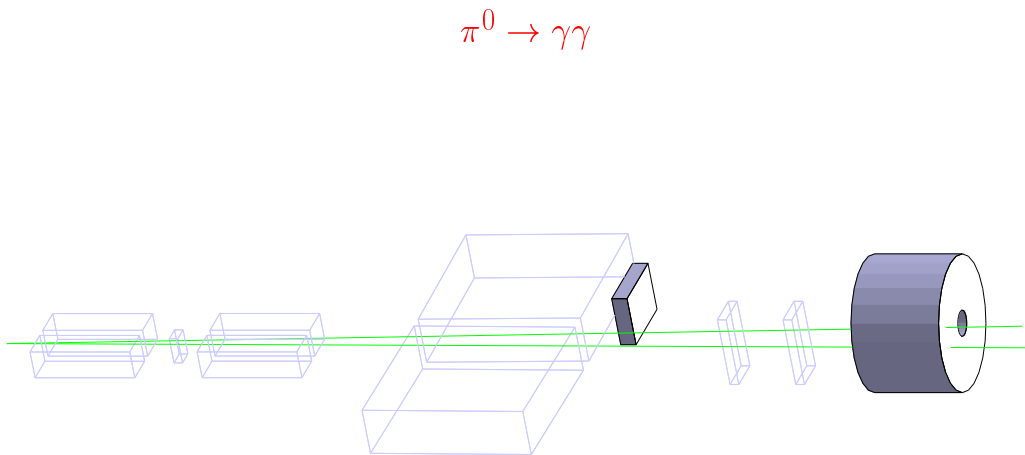
$$\pi^0 \to \gamma\gamma$$

Figure 21: Sketch of a $\pi^0 \to \gamma\gamma$ decay event
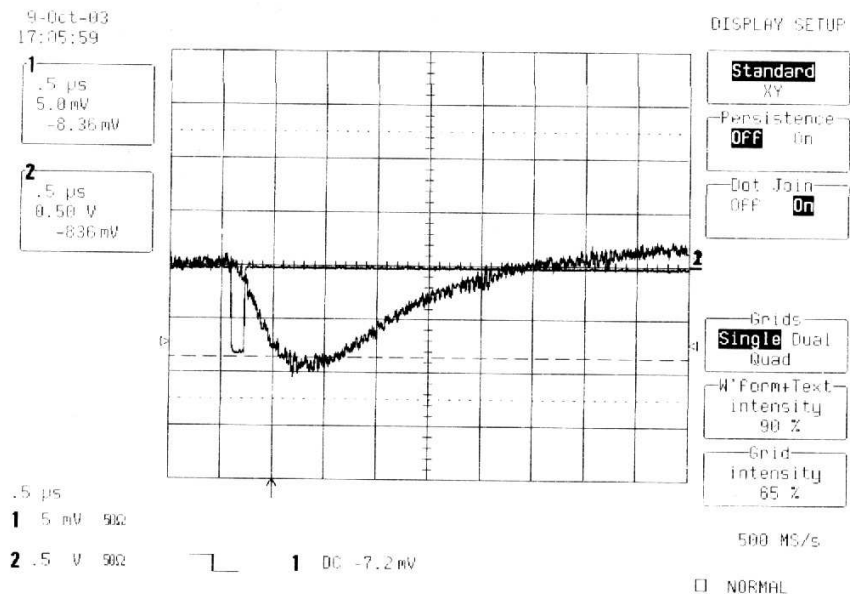
Figure 22: Response signal of a typical block
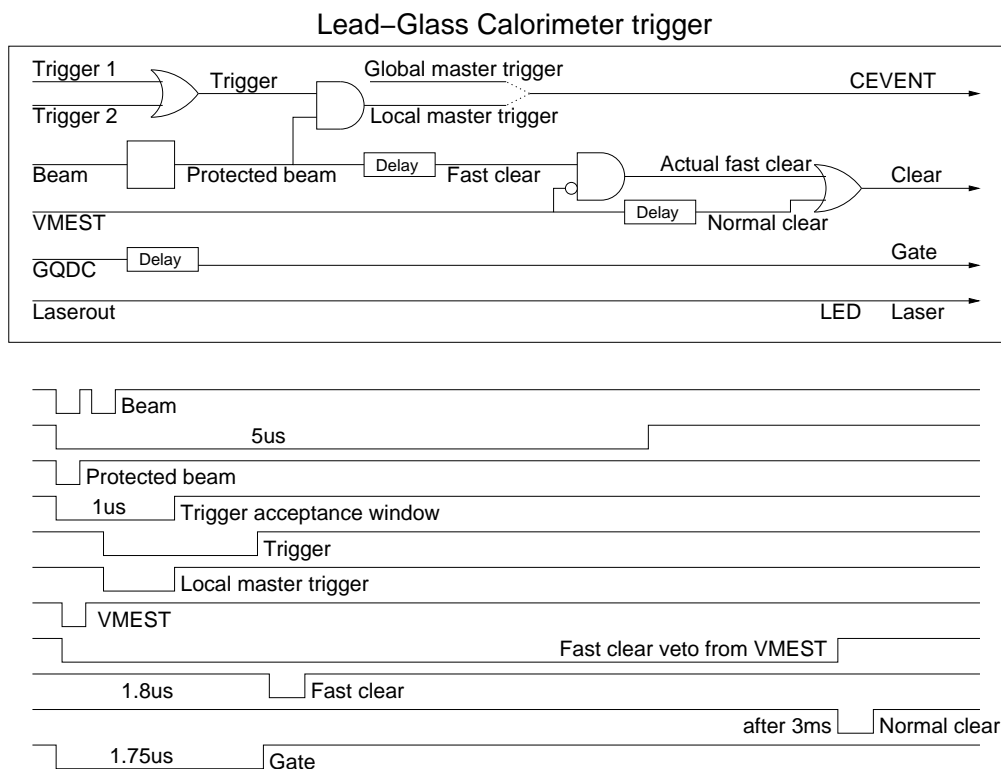
Lead–Glass Calorimeter trigger

Figure 23: LGC trigger logic

The signal labeled *Beam* is the raw trigger signal of NA49, which was previously mentioned. Often more than one beam particles follow closely each other, therefore a filtering of *Beam* signal is necessary, which results in the signal *Protected beam*. It is obtained in such a way that, by the first up-running edge of *Beam* signal, a $5\mu s$ long signal is generated immediately, which is delayed by 150ns, negated, and coincided with the original *Beam* signal. This method, intuitively, picks out the first *Beam* signal in a $5\mu s$ window, which prevents multiple rapid triggering of the DAQ computer. When the LGC trigger unit is switched on, the signal *CEVENT* means an LGC trigger signal, which starts the DAQ computer, and the analog-digital conversion of the signals of LGC begins. The computer verifies the starting of data acquisition by the signal *VMEST*. If for some reasons, the *VMEST* signal does not appear (the starting of DAQ has failed), the signal *Fast clear* resets the DAQ. Otherwise, the signal *VMEST* vetoes the *Fast clear*, and the DAQ is only reset after 3ms by the *Normal clear*, when the AD conversion is already finished.

3.2   Relative calibration of the LGC channels

First of all, a labeling convention is needed for the channels. Channels are indexed by their row and column numbers. The zeroth row is defined to be the upmost row, the zeroth column is defined to be the leftmost column, if one looks onto the back of LGC (i.e. one is facing the target). There is also an other label in use, which is called the channel number. The conversion between the coordinates (#row, #column) and the label #channel is defined by the one-to-one and onto relation #channel = #column|8 + #row · 8 + (#column ÷ 96) · 96, where ÷ means integer division, | means modulus.

The first step in calibration is to measure the pedestals of each analog-digital converter. The AD converters are 12 bit flash converters. The incoming signal of each channel is AD converted in such a way, that both the signal and the approximately 1/8 of the signal is AD converted. The value of the former conversion is called the *high ADC*, the value of the latter conversion is called the *low ADC*. Thus, the total dynamical range is approximately 9 times wider than the dynamical range of high ADC-s, because if the high ADC of a signal is in saturation, the low ADC of the signal can be used. As the high and low ADC-s are obtained with two different AD converters for each channel, pedestals for both the high and low ADC-s have to be obtained, channel-by-channel. Furthermore, the conversion factor between the low and high ADC-s (which is approximately 8) has to be obtained for each channel, to be able to unify the high and low ADC scales.

3.2.1   Calculating the pedestals

The pedestals are calculated for each experimental run individually, because it turned out, that the pedestals may slip somewhat (of course, very slowly). They are calculated via Gaussian fit for the high and low energy (ADC) spectrum of each channel.

For demonstration, we show the energy (high ADC) spectrum of specific channels in *figure 24* (Gaussian pedestal fits are also drawn). This series of data was recorded by using the self-trigger of LGC. The target tank was full (liquid hydrogen was used), thus physical events were expected. As one can see, the energy spectrum of those channels, which are nearer to the nominal beam line, develop a tail. This effect shows the natural fact that more high-energetic particles traverse the volume of LGC near the beam line than on the other side.

3.2.2   Calculating the high/low gains

The high/low gains are also calculated for each experimental run separately.

The histogram of high/low responses (with subtracted pedestals) are recorded for each channel. The place of the maximum of the histogram is assigned to the value of the high/low gain. (There is no point in Gaussian fitting, as these histograms turned out to be very sharp, much sharper than a Gaussian distribution.)

3.2.3   Relative calibration of LGC channels with cosmic rays

After the high and low pedestals, and the high/low gains are obtained, the energy value of a response can be reconstructed up to a calibration factor, in each channel. In the rest of this subsection, the relative calibration of LGC channels will be discussed. If the relative calibration factors are known, the energy value of a response can be calculated, up to a global scale factor.
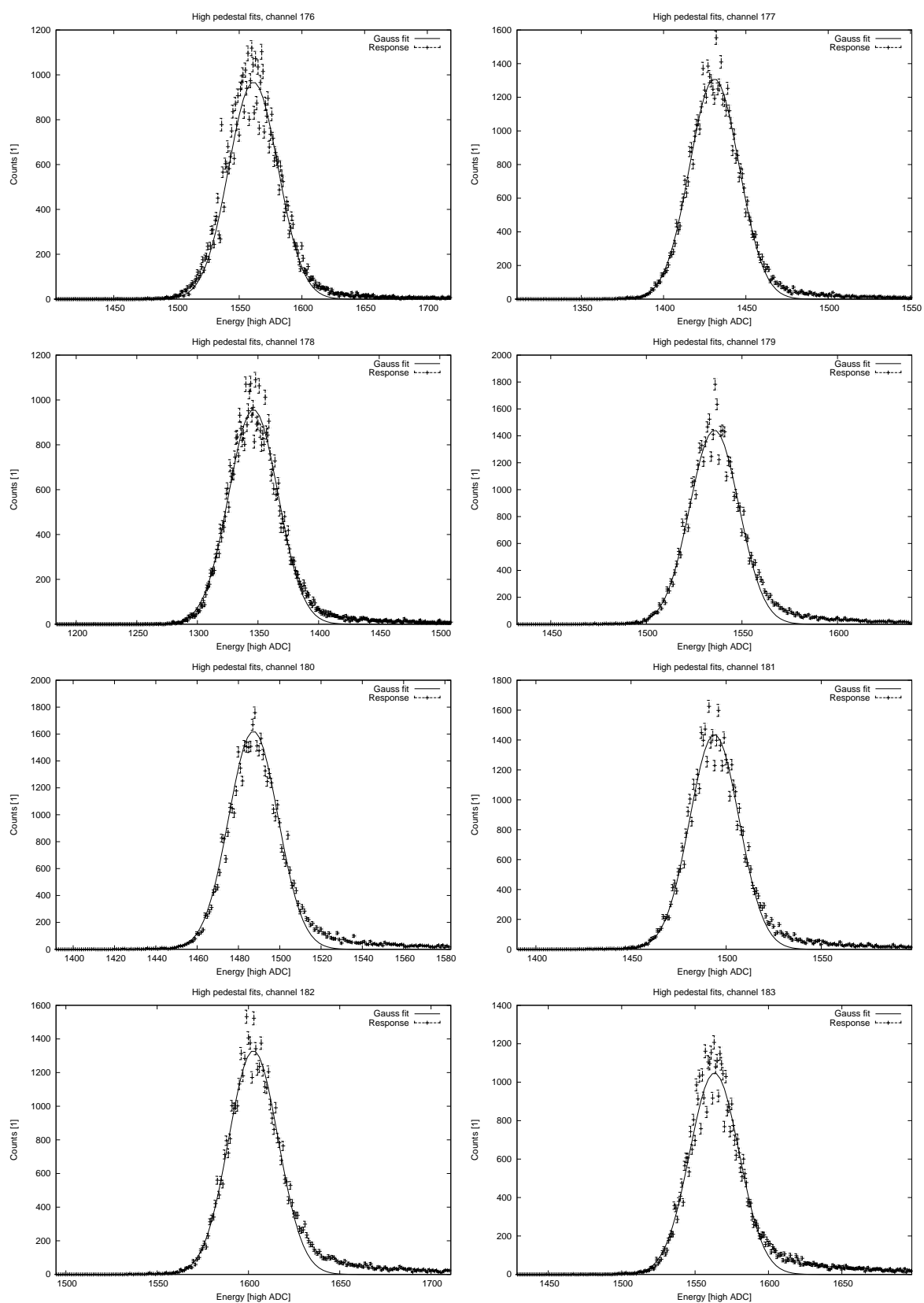
Figure 24: LGC channel histograms in row 10, from column 8 to 15, with Gaussian pedestal fits

This scale factor can be fixed by measuring the mass peak of the π^0 particle, which will be discussed in the next subsection.

As one can see in *figure 19, 20*, there is a shift device built on the concrete block, under the LGC detector. With this shift device, the LGC can be shifted by 0, 1, 2 or 3 channels, away from the beam line. This facility was built for the relative calibration of channels in a row, in the following way. One records an amount of events with LGC, by using a trigger which is independent from LGC (i.e. one of the original trigger setup of NA49). Then, one records the same amount of events, with the same setup, when the LGC is shifted by 1 channel. After the shifting, the position of a channel with coordinates ($\#$row, $\#$column) is taken by the channel with coordinates ($\#$row, $\#$column $+ 1$). Therefore, the energy spectrum, measured by these channels in this two situation, can be assigned to each other, thus a relative calibration can be obtained between each neighboring channel in a row. It follows, that the relative calibration factors in each row can be obtained, which can be rescaled to have 1 as relative calibration factor for each channel with coordinates ($\#$row, 0).

Unfortunately, this process could not be carried out, due to the following technical obstruction. One of the Main-TPC-s had some technical problems in the beginning of the run period, therefore the beam could not be used for several days, as maintenance was going on. After the maintenance, there remained not enough time for calibration. A new method was needed. The following method, suggested by the author, was used finally, which is based on cosmic ray measurements. In cosmic ray measurements, the self-trigger of LGC is used.

The cosmic rays reach the surface of Earth with a homogeneous flux, due to the fact that these particles (which are mainly muons) come from far. Unfortunately, the cosmic muons themselves are not detectable by LGC, because a typical cosmic muon is minimum-ionizing, therefore it does not leave an amount of energy higher than the noise threshold in LGC. Fortunately, the muons do decay frequently enough, and the electrons originating from the decay of cosmic muons turned out to be detectable by LGC.[9] Cosmic ray events are shown in *figure 25*.[10] The rate of cosmic ray events turned out to be about $0.2\frac{1}{\text{s}}$.

We use the fact, that given any fixed energy threshold, the flux of those cosmic particles, which have energy greater or equal to this threshold, is horizontally homogeneous. (This means, that all cosmic particles come from far, independently of their energy, i.e. of their physical formation.) Therefore, given a fixed row of LGC, the probability of getting a cosmic hit over a global energy threshold in a channel obeys binomial probability rule. Let $p(n, k)$ be the probability of the event, that a given channel in the row got k hits above the threshold, while the total hits of this kind in the row is n. Then $p(n, k) = \binom{n}{k} p^k (1-p)^{n-k}$ with $p := \frac{1}{N}$, where N denotes the number of those channels in the row, which are operating properly (i.e. not dead). Thus, the expected value of hits above the threshold in each channel is $\frac{n}{N}$, while the relative fluctuation is $\frac{\sqrt{N-1}}{\sqrt{n}}$.

We can use the above facts for relative calibration of channels in a row. Let us fix a row with identity number $\#$row. We record the energy (ADC) spectrum of each channel in the

---

[9]Electrons are detectable as they are not minimum-ionizing, because of high amount of energy loss via bremsstrahlung.

[10]The first two events are most likely to be hits of electromagnetic particles (e.g. electrons from muon decay), as they develop a tail only of about 40cm (this approximately corresponds to the typical length of an electromagnetic shower in lead glass). The second two events are most likely to be hits of high energetic hadronic particles (e.g. protons with energy about a few 100GeV-s), as their tails develop much longer. Events of the former kind are quite frequent, while events of the latter kind are quite rare.
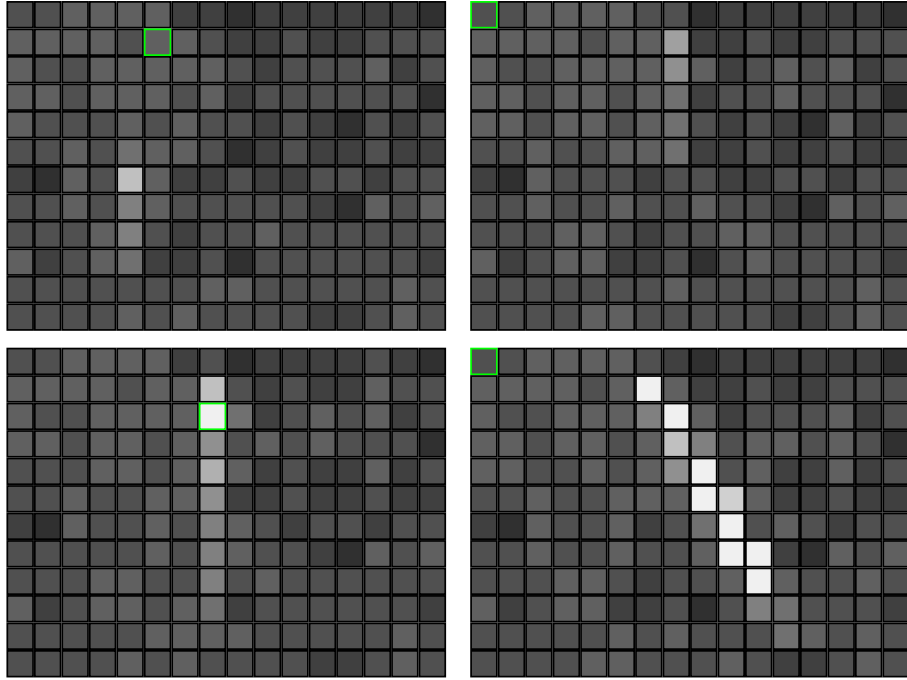
Figure 25: LGC event display: cosmic ray events

row, for cosmic ray runs. We introduce a threshold, e.g. $4\sigma_{\#\mathrm{row}}$, where $\sigma_{\#\mathrm{row}}$ is the greatest pedestal width in the row (by pedestal width, we mean the pedestal width for the high ADC-s). Let us denote this threshold by $k_{\#\mathrm{row}}$. We look for the channel in the row, which has the lowest number of cosmic hits with energy above the ADC value $k_{\#\mathrm{row}}$. Let us denote this count by $C_{\#\mathrm{row}}$. Then, we raise the threshold for every channel in the row independently, in order to get the same counts above the thresholds as $C_{\#\mathrm{row}}$, in each channel. Let us denote the thresholds, obtained by this method, by $k_{(\#\mathrm{row},\#\mathrm{column})}$ for the channels $(\#\mathrm{row}, \#\mathrm{column})$. The homogeneous flux argument implies, that these threshold values correspond to the same physical energy in the given row (up to the error of counts), thus a relative calibration can be obtained.

There is a further source of error for the counts, which originates from the fluctuation of the number of photo electrons emitted from the photo cathode of the corresponding vacuum photo triode. It is a well known fact, that the fluctuation of counts, caused by the previous effect, in a given energy range is the square root of the counts in the given energy range. This fluctuation (which corresponds to $\sqrt{\frac{n}{N}}$) is independent from the spatial fluctuations of cosmic hits above the energy threshold (the former is only due to the photo triodes of the measuring apparatus). Therefore, the total relative fluctuation of the measured counts is $\frac{\sqrt{2N-1}}{\sqrt{n}}$ with the previous notation, as the square of the standard deviation of counts, arising from this two effect, can simply be added.

To obtain the error of the calibration factors, we have to investigate the propagation of the above error. The spectrum of the cosmic rays is known to be of the form $E \mapsto C \cdot E^{-2.7}$ on the relevant range (i.e. $1-100\mathrm{GeV}$), for a given normalization factor C. Let us take a threshold E_0, then $\int_{E_0}^{\infty} \mathrm{d}E C \cdot E^{-2.7} = \frac{1}{1.7} C \cdot E_0^{-1.7}$, which is the number of the counts over E_0. When applying

our method, we fix the counts, and want to obtain the lower threshold, thus we are interested in the error of the lower threshold, arising from the error of counts. As the counts for a threshold E_0 correspond to $\frac{1}{1.7} C \cdot E_0^{-1.7}$, we have that the relative error of the threshold is $\frac{1}{1.7}$ times the relative error of counts.[11] Thus, the relative error of the thresholds correspond to $\frac{1}{1.7} \frac{\sqrt{2N-1}}{\sqrt{n}}$. As the relative calibration factors are quotients of thresholds, one can calculate the error of the relative calibration factors: the corresponding relative calibration factor is $\frac{k_{(\#\text{row},0)}}{k_{(\#\text{row},\#\text{column})}}$, and its relative error is $\frac{2}{1.7} \frac{\sqrt{2N_{\#\text{row}}-1}}{\sqrt{n_{\#\text{row}}}}$, where $N_{\#\text{row}}$ is the number of properly operating channels in the given row, and $n_{\#\text{row}}$ is the sum of total counts in the row, which are over the final thresholds.

The relative errors of calibration factors in the rows, obtained by a few days of cosmic ray runs, can be bounded by 3%.

The vertical relative calibration was done by a similar method, discussed below.

The zeroth column is more than 3m far from the beam line. One can assume, that the flux of particles from the target, arriving into this column, is homogeneous. The systematic error of this assumption is estimated to be about 5%. The statistical error (with the previous method) is estimated to be about 4%. Thus, the total error of vertical relative calibration is about 10%. This is not satisfactory, but it is enough to be able to see the π^0 mass peak. It is planned that, in the summer of 2004, vertical calibration will be redone by using cosmic ray calibration, as in the horizontal case.

3.3 The π^0 mass peak

π^0 particles are detectable with LGC, by detecting the two gamma photons originating from a π^0 decay. The energy of the gamma photons can be determined from the LGC responses. The angle of decay between the two gamma photons can be determined (with good approximation) by dividing the distance of the two gamma hits on the face of LGC by 17.77m. Four π^0 candidate events are shown in *figure 26*.

3.3.1 Kinematics of $\pi^0 \rightarrow \gamma\gamma$ decays

This part is devoted to kinematical studies of $\pi^0 \rightarrow \gamma\gamma$ decays, in order to obtain some a priori estimates on expected π^0 detection rates with LGC. The kinematical quantities, which will be used below, are understood to be in an Einstein-synchronized laboratory frame, if not specified otherwise.

If a particle with mass M decays into two particles with mass m, then

$$M = \sqrt{2e_1 e_2 + 2m^2 - 2\cos\alpha \sqrt{(e_1^2 - m^2)(e_2^2 - m^2)}},$$

where e_1 and e_2 is the energy of the two resultant particle, and α is the angle between the momentum of the two particles (angle of decay). In the case of $m = 0$, $M = \sqrt{e_1 e_2} 2 \sin\frac{\alpha}{2}$ is true. Therefore, in the case of $\alpha \ll 1$, $M \approx \sqrt{e_1 e_2} \alpha$ is valid.

In the case of LGC, the minimal measurable angle is 0.0095rad, the maximal measurable angle is 0.0883rad, so the approximation of small angles is valid with the relative error limit

---

[11] The error propagation can also be obtained directly from the recorded energy (ADC) histograms (without assuming any theoretical shape for the energy spectrum), provided that the amount of recorded data is large enough.
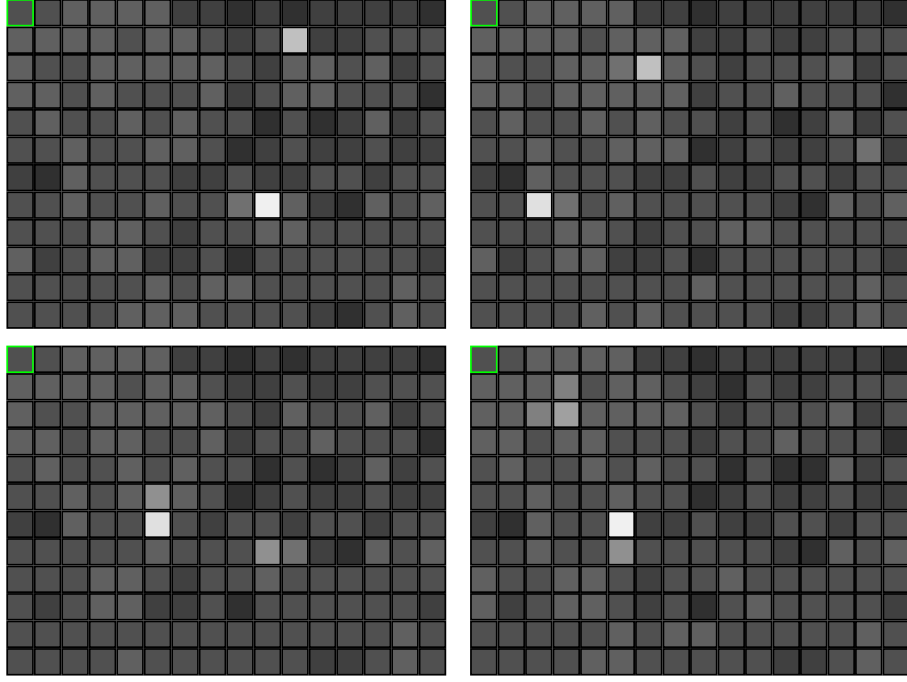
Figure 26: LGC event display: π^0 candidate events

0.000325, in the above approximation. The cuts in angle measurements will impose cuts on the energy of such measurable π^0 particles, when the two gamma photon hits are distinguishable (i.e. both hit LGC, but they do not hit the same channel). This will be investigated below.

Let us denote the angle between the axis of decay, and a fixed axis (in rest frame) by ϑ. Then, in the boosted laboratory frame the angle of decay is given by

$$\alpha_\omega(\vartheta) = \arccos\left(\frac{\sinh^2\omega - \cos^2\vartheta\cosh^2\omega - \sin^2\vartheta}{\sqrt{(\sin^2\vartheta + (\sinh\omega - \cos\vartheta\cosh\omega)^2)(\sin^2\vartheta + (\sinh\omega + \cos\vartheta\cosh\omega)^2)}}\right),$$

where ω is the rapidity of the π^0 particle in the laboratory.

The minimal value of the angle of decay is determined by the map $\omega \mapsto \arccos\left(1 - \frac{2}{\cosh^2\omega}\right)$. This gives an absolute kinematical cut for π^0 detection, at the lower energies, as the minimal angle of decay has to be smaller than 0.0883rad. Thus, the cut at lower energies is 3.812524 in rapidity, that is 3.1GeV in π^0 energy.

The expected value of the angle of decay for given rapidity ω is $\frac{1}{2}\int\limits_0^\pi \alpha_\omega(\vartheta)\sin\vartheta\mathrm{d}\vartheta$. This integral cannot be calculated explicitly, but one can make a good approximation of the expected angle above about rapidity 3.0, that is above about 1.5GeV π^0 energy. The approximation is based on the fact, that the integrand of the above integral is nearly flat, if the rapidity is high enough (see *figure 27*), thus the integrand can be substituted by the maximal value of it. Namely, the expected angle with this approximation is given by the map $\omega \mapsto \frac{\pi}{2}\arccos\left(1 - \frac{2}{\cosh^2\omega}\right)$. The relative error of this approximation of the expected angles at rapidity 3.0 is 0.048921 and at rapidity 4.263 is 0.014013, which were calculated by numerical integration. By investigating the error propagation, one can find, that the relative error in rapidity, which corresponds to the previous approximation error, is 0.001988 at rapidity 3.0 and is 0.000014 at rapidity 4.263.

The relative error of π^0 energy arising from the previous approximation error is 0.005935 at rapidity 3.0 and is 0.000060 at rapidity 4.263, therefore this approximation is affordable.
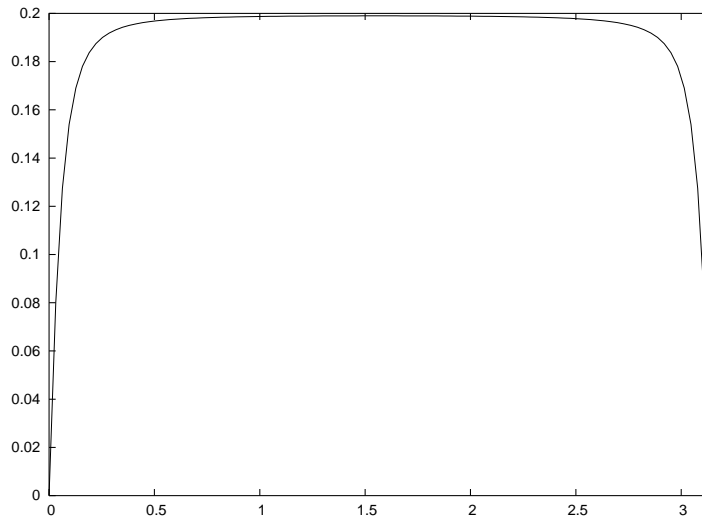

Figure 27: The integrand, at rapidity 3.0

As a consequence of the cuts in angle measurements, an average measurable π^0 has a characteristic energy greater than 4.8GeV and lesser than 44.6GeV, if we require the two gamma hits to be distinguishable.

The maximal value of the angle of decay at given rapidity is given by the constant map $\omega \mapsto \pi$, thus it does not imply an absolute kinematical cut at higher energies, for π^0 detection. However, an upper kinematical cut can be determined from the expected value of the angle of decay, as the standard deviation of the angle of decay drops down at higher energies. Namely, numerical integration show, that the standard deviation of the angle of decay at rapidity 6.4 (at 40.6GeV π^0 energy) becomes 0.013619rad, which is small (it corresponds approximately to the minimal measurable angle). By requiring the expected value to be greater than the minimal measurable angle, one gets the upper kinematical cut: the two gamma hits are not expected to be distinguishable above 44.6GeV π^0 energy.

The minimal energy, when the two gamma photons can hit the same channel, is at rapidity 6.042753, that is at 28.4GeV π^0 energy.

A Monte Carlo simulation was written by the author, in order to get an estimate on the expected rate of detectable π^0 particles with LGC, by using the original (n+p) trigger system. The simulation was based on previously recorded TPC-track data of charged particles. These charged particles are known to be mainly (in about 90%) π^+ and π^- particles, from previous surveys. By assuming isospin symmetry, one can interpret their momenta (which are determined, and extrapolated to the target from TPC-track data) as π^0 momentum data. Given this system of momentum data, one can simulate the decay of π^0 particles, possessing these momenta.[12] The Monte Carlo simulation, based on this idea, predicts the following rates of detectable particles for LGC:

1. the probability of recording such an event with the n+p trigger system, which contains a detectable pair of gamma photons originating from π^0 decay, is 8.3%;

---

[12]Here we have to assume, that the acceptance for $\pi^\pm$ detection is about 100%.

2. the probability of recording such an event with the n+p trigger system, which contains a single detectable pair of gamma photons originating from π^0 decay, is 7.4%;

3. the probability of recording such an event with the n+p trigger system, which contains a single detectable pair of gamma photons originating from π^0 decay while no other detectable particle traverse LGC, is 6.0%;

4. the mean energy of detectable π^0 particles is 9.8GeV.

3.3.2   Experimental results

The main result of the first measurements with LGC is the π^0 mass peak in the spectrum of twophoton events.

The results are shown in *figure 28*. These plots were obtained by the analysis of about 80000 events. About half of them were recorded with the n+p trigger, about half of them were recorded with the LGC self-trigger. (One gets similar peaks, of course, by processing only the n+p trigger events, or only the LGC events.) As one can see, the resolution of the detector could be better (the π^0 mass peak is too wide). This is due to the fact, that the vertical calibration factors have about 10% errors.

For comparison, we also present the mass spectrum predicted by the Monte Carlo simulation in *figure 29*. In order to be more realistic, the granularity of LGC was taken into account in the simulation, furthermore 15% uncertainty in energy measurements was assumed.
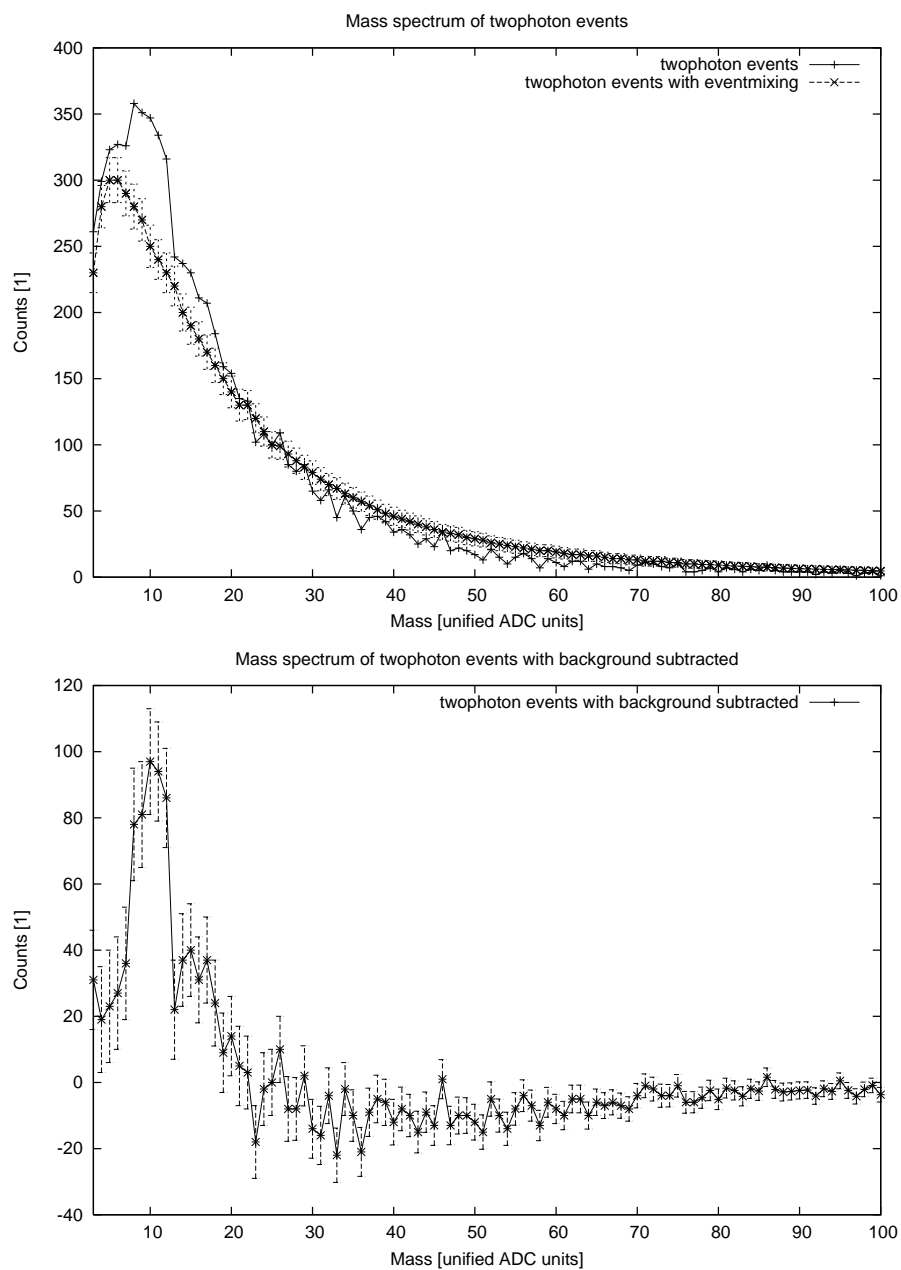
Figure 28: The π^0 mass peak
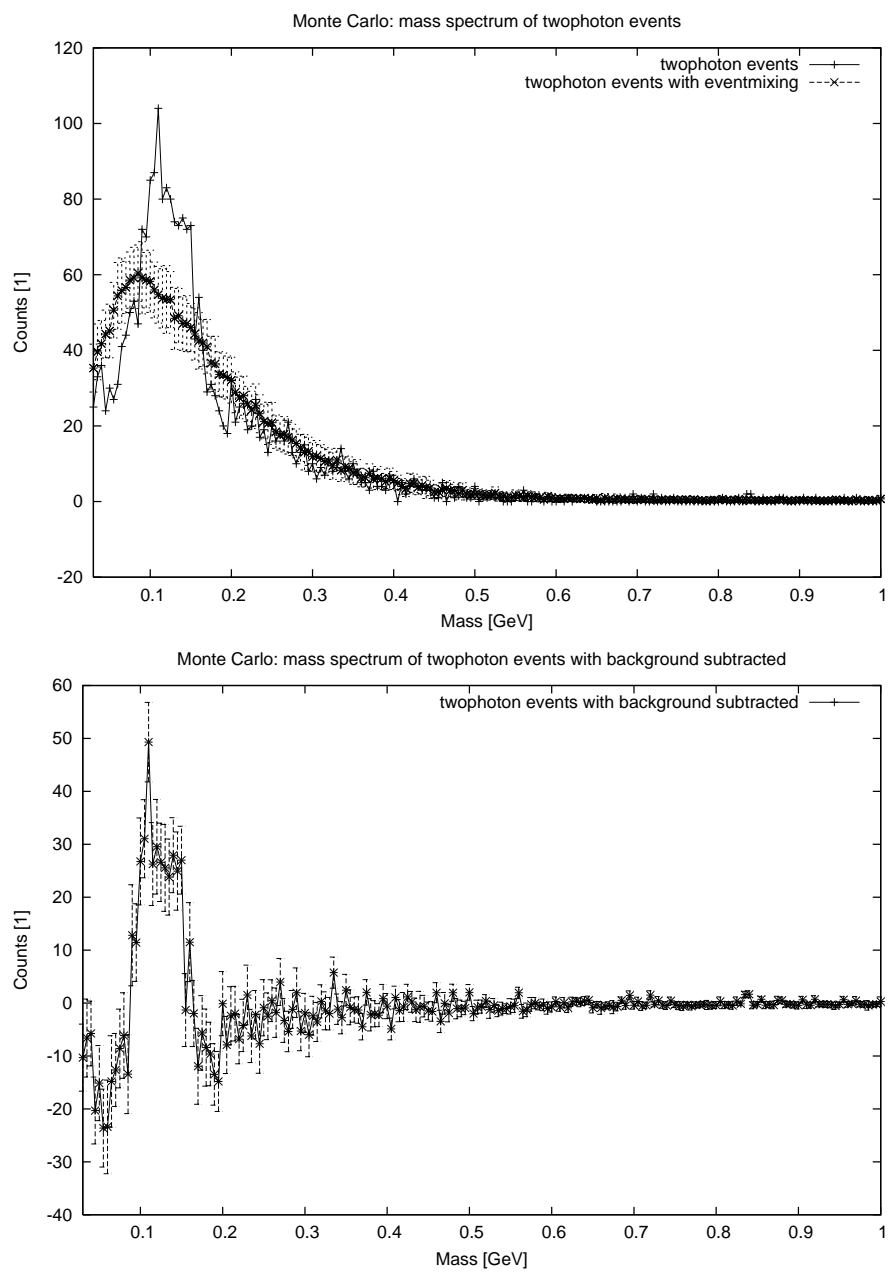
Figure 29: The π^0 mass peak from Monte Carlo simulation

4   Concluding remarks

In the first part, results of homogeneity and linearity tests of the HF calorimeter (which were carried out in June-August 2003, at SPS accelerator, CERN) were presented. As a summary, we can state that the inhomogeneity of the energy response in space can be bounded by 10%. The linearity of response (which was measured in the energy scale $50 - 300 GeV$) is not so good at lower energies. The error of linearity for the electromagnetic part of the measured towers is about 6% and for the hadronic part of the measured towers is about 12%.

In the second part, results of the first measurements with the LGC (which were carried out in October 2003, at experiment NA49, at SPS accelerator, CERN) were presented. The main result is the π^0 mass peak, which is the first physical effect, measured with LGC.

Acknowledgements

5   Appendix (about software works)

All the results in this paper were obtained by various analysis software, written by the author in various programming languages (C, GNUplot, C++, ROOT etc.). The total amount of code is about 5000 lines for HF and is about 9000 lines for LGC. Most of the software were used for debugging the data acquisition system, monitoring the quality of the acquired data etc. The sources are available under the following URL-address:

`http://szofi.elte.hu/project/la_thesis`

Some of the analysis software (e.g. the pedestal fitter for LGC etc.) is likely to be used in future runs, but they are too sophisticated to present here. Some of them are written in compound languages: C + GNUplot + Shell, where sometimes such programs run, which are written by other programs, up to 2-3 level.

Most probably the Monte Carlo simulation, written for the LGC, will be used for works in future. As it is not so sophisticated, my supervisor suggested to present part of the simplified pseudocode of it, here. (The base language is C.)

Monte Carlo simulation for LGC

The program reads an ASCII file (`TrackDump.dat`), which is a dump of reconstructed track data of the TPC-s of NA49. Namely, the file contains lines of the following format:

`event charge px py pz x y z tanl phi`

Here `event` is an event identity number, `charge` means the charge (calculated from the track reconstruction), while `px,py,pz` are the momentum coordinates of the given particle (extrapolated to the target), determined from Vertex-TPC track data (the Vertex-TPC-s are in magnetic field). After the Vertex-TPC, the particles enter the Main-TPC, where there is no magnetic field, thus the tracks are straight lines. The coordinates `x,y,z` mean the start point of the straight line, while `tanl` and `phi` encode the inclination of the straight line. The event identity `event` starts from 0, and increases by 1 at each event.

```
... Header includes etc. ...

// The structure for a particle hit in LGC
// (Energy, horizontal and vertical hit  coordinates):
typedef struct
{
 double E;
 double X;
 double Y;
}
Part_t;

// The structure for momentum and coordinate 3-vectors:
typedef struct
{
```

```
 double x;
 double y;
 double z;
}
Vector_t;

// The structure for reconstructed tracks
// (charge, momentum at target, the start point of Main-TPC track,
// and the inclination parameters of the Main-TPC track):
typedef struct
{
 int charge;
 Vector_t P;
 Vector_t R;
 double tanl;
 double phi;
}
Track_t;

// The structure for an event
// (event identity number, the number of tracks, the array of tracks):
typedef struct
{
 int event;
 int numTrack;
 Track_t *T;
}
Event_t;

// This is the length function of 3-vectors:
double Length(Vector_t *V)
{
 ...
}

// This function reads the two polar angles of the pi0 decay axis in rest
// frame, the 3-momentum of pi0 in laboratory frame, and dumps the
// momenta of the two resultant gamma photons in laboratory frame into
// a pair of momentum  variables:
void Gamma(double theta, double phi, Vector_t *P, Vector_t *p1, Vector_t *p2)
{
 ...
}

// Determines the angle of decay of two particle hits in LGC,
// (here, granulation of LGC can be taken into account):
double angle(Part_t *p1, Part_t *p2)
```

```
{
 ...
}

// Determines that whether a momentum can be extrapolated from the target
// to the volume of LGC (returns 1 if 'yes', 0 if 'no'):
int inLGC(Vector_t *p)
{
 ...
}

// The X impact point coordinate of a particle momentum,
// linearly extrapolated to the face of LGC:
double XMomToLGC(Vector_t *p)
{
 ...
}

// The Y impact point coordinate of a particle momentum,
// linearly extrapolated to the face of LGC:
double YMomToLGC(Vector_t *p)
{
 ...
}

// Determines that whether Main-TPC track can be extrapolated
// to the volume of LGC (returns 1 if 'yes', 0 if 'no'):
int leadsTrack(Track_t *T)
{
 ...
}

// The X impact point coordinate of a Main-TPC track on the face of LGC:
double XTrack(Track_t *T)
{
 ...
}

// The Y impact point coordinate of a Main-TPC track on the face of LGC:
double YTrack(Track_t *T)
{
 ...
}



// Main body of the program:
int main(int argc, char *argv[])
```

```
{

// File variable for reading TrackDump.dat:
FILE *file;

int event, eventold;
int track;
int charge;
double px,py,pz;
double x,y,z;
double _tanl,_phi;
int i;
int p;
Vector_t p1,p2;
double rnd;
double theta,phi;
int Event;
char buff[256];

// Arrays for storing events, and particle impacts:
Event_t *eventstore;
Part_t *twophotonstore[2];
Part_t *particle;

int NumEvents;
int twophnum;

// Reading lines of TrackDump.dat, determining the number of events
// (NumEvents):
file=fopen("TrackDump.dat", "r");
NumEvents=0;
while ( feof(file)==0 )
{
 if ( fgets(buff, 256, file)==NULL ) { break; }
 sscanf(buff, "%d %d %lg %lg %lg %lg %lg %lg %lg %lg",
      &event, &charge, &px, &py, &pz, &x, &y, &z, &_tanl, &_phi);
 if ( NumEvents==0 ) { eventold=event-1; }
 if ( eventold!=event ) { NumEvents++; }
 eventold=event;
}
fclose(file);

... Initializing, allocating memory for arrays etc. NumEvents is
    needed e.g. here. ...

// Reading lines of TrackDump.dat, determining the number of tracks at
// each event:
```

```
file=fopen("TrackDump.dat", "r");
i=0;
while ( feof(file)==0 )
{
 if ( fgets(buff, 256, file)==NULL ) { break; }
 sscanf(buff, "%d %d %lg %lg %lg %lg %lg %lg %lg %lg",
     &event, &charge, &px, &py, &pz, &x, &y, &z, &_tanl, &_phi);
 if ( i==0 ) { eventold=event-1; i=1; }
 if ( eventold!=event )
 {
   eventstore[event].event=event;
   eventstore[event].numTrack=0;
 }
 eventstore[event].numTrack++;
 eventold=event;
}
fclose(file);

// Reading lines of TrackDump.dat, obtaining track data:
file=fopen("TrackDump.dat", "r");
i=0;
while ( feof(file)==0 )
{
 if ( fgets(buff, 256, file)==NULL ) { break; }
 sscanf(buff, "%d %d %lg %lg %lg %lg %lg %lg %lg %lg",
     &event, &charge, &px, &py, &pz, &x, &y, &z, &_tanl, &_phi);
 if ( i==0 ) { eventold=event-1; i=1; }
 if ( eventold!=event )
 {
   eventstore[event].T=
       (Track_t *)calloc(eventstore[event].numTrack, sizeof(Track_t));
   track=0;
 }
 eventstore[event].T[track].charge=charge;
 eventstore[event].T[track].P.x=px;
 eventstore[event].T[track].P.y=py;
 eventstore[event].T[track].P.z=pz;
 eventstore[event].T[track].R.x=x;
 eventstore[event].T[track].R.y=y;
 eventstore[event].T[track].R.z=z;
 eventstore[event].T[track].tanl=_tanl;
 eventstore[event].T[track].phi=_phi;
 track++;
 eventold=event;
}
fclose(file);
```

```
// The core of the Monte Carlo simulation:
twophnum=0;
for ( event=0 ; event<NumEvents ; event++ )
{

 // Number of particle hits in LGC during an event:
 p=0;

 // Fetching randomly an other event (the charged particle tracks,
 // crossing LGC, are obtained from this event):
 rnd=drand48();
 Event=(int)(rnd*NumEvents);
 for ( track=0 ; track<eventstore[Event].numTrack ; track++ )
 {
  // If the Main-TPC track leads to LGC:
  if ( leadsTrack(&eventstore[Event].T[track])==1 )
  {
   // As particles, having Main-TPC tracks, are mainly pi+ and pi-
   // (i.e. charged hadronic) particles, the energy, deposited in LGC,
   // is taken to be the 1/3 of the real energy
   // (hadronic shower leakage is taken into account this way):
   E=Length(&eventstore[Event].T[track].P)/3.0;
   // Ultrarelativistic limit is assumed in the above line.
   // Let the energy threshold, for considering a response as a
   // particle hit, to be 1GeV:
   if ( E>1.0 )
   {
    // Filling the store of particle hits on LGC:
    particle[p].E=E;
    particle[p].X=XTrack(&eventstore[Event].T[track]);
    particle[p].Y=YTrack(&eventstore[Event].T[track]);
    p++;
   }
  }
 }

 // Simulating pi0 decays with momenta from original event:
 for ( track=0; track<eventstore[event].numTrack ; track++ )
 {

  // Faking a momentum for pi0 particle from the momentum of a
  // pi- particle (isospin symmetry is assumed): the fake pi0 momentum
  // is defined to be eventstore[event].T[track].P if
  // the particle charge is negative, i.e.
  // when eventstore[event].T[track].charge==-1.
  if ( eventstore[event].T[track].charge!=-1 ) { continue; }
```

```
// Generating random polar direction for axis of decay in rest frame:
rnd=drand48();
theta=acos(2.0*rnd-1.0);
rnd=drand48();
phi=2.0*M_PI*rnd;

// The decay of the corresponding pi0: the momenta of the gamma
// photons are stored in p1 and p2:
Gamma(theta, phi, &eventstore[event].T[track].P, &p1, &p2);

// If the momentum of the first gamma photon leads to LGC:
if ( inLGC(&p1)==1 )
{
 // As photons are electromagnetic particles, their total
 // energy is measured by LGC:
 E=Length(&p1);
 // Let the energy threshold, for considering a response as a
 // particle hit, to be 1GeV:
 if ( E>1.0 )
 {
  // Filling the store of particle hits on LGC:
  particle[p].E=E;
  particle[p].X=XMomToLGC(&p1);
  particle[p].Y=YMomToLGC(&p1);
  p++;
 }
}
// If the momentum of the second gamma photon leads to LGC:
if ( inLGC(&p2)==1 )
{
 // As photons are electromagnetic particles, their total
 // energy is measured by LGC:
 E=Length(&p2);
 // Let the energy threshold, for considering a response as a
 // particle hit, to be 1GeV:
 if ( E>1.0 )
 {
  // Filling the store of particle hits on LGC:
  particle[p].E=E;
  particle[p].X=XMomToLGC(&p2);
  particle[p].Y=YMomToLGC(&p2);
  p++;
 }
}
}

// If the number of particle hits on LGC is 2, store the hits:
```

```
 if ( p==2 )
 {
  twophotonstore[twophnum][0].E=particle[0].E;
  twophotonstore[twophnum][0].X=particle[0].X;
  twophotonstore[twophnum][0].Y=particle[0].Y;
  twophotonstore[twophnum][1].E=particle[1].E;
  twophotonstore[twophnum][1].X=particle[1].X;
  twophotonstore[twophnum][1].Y=particle[1].Y;
  twophnum++;
 }

}


... Now the store of twohits (twophotonstore[twophnum]) can be processed.
    Histograms etc. can be calculated
    (e.g. double angle(Part_t *, Part_t *) is used here). ...

... Results are stored. ...

... Memory freed. ...

}
```

References

[1] A. Beer, G. Critin, G. Schuler: *Design of a Fast Gated Charge Integrating Front End for Use in High Density CAMAC and Fastbus Modules*; Nuclear Instruments and Methods in Physics Research, 1985, A234, p. 294-301

[2] P. Gorodetzky, D. Lazic, G. Anzivino, E. Chiavassa, A. Contin, G. Dellacasa, N. Demarco, R. De Salvo, M. Gallio, P. Guaita, K. F. Johnson, P. Juillot, M. Lundin, M. Marino, A. Musso, A. Piccotti, E. Scomparin, E. Vercellin: *Quartz Fiber Calorimetry*; Nuclear Instruments and Methods in Physics Research, 1995, A361, p. 161-179

[3] P. W. Jeffreys, M. Akrawy, G. T. J. Arnison, J. R. Batley, K. W. Bell, R. M. Brown, A. A. Carter, J. R. Carter, W. M. Evans, N. I. Geddes, C. N. P. Gee, W. R. Gibson, M. J. Goodrick, P. Kyberd, G. N. Patrick, M. D. Rousseau, R. A. Sansum, B. J. Saunders, M. Sproston, C. P. Ward: *Development Studies for the OPAL Endcap Electromagnetic Calorimeter Using Vacuum Photo Triode Instrumented Lead Glass*; Nuclear Instruments and Methods in Physics Research, 1990, A290, p. 76-94